IEEE Access
Multidisciplinary | Rapid Review | Open Access Journal

Received September 10, 2021, accepted September 16, 2021, date of publication September 20, 2021,
date of current version October 5, 2021.

Digital Object Identifier 10.1109/ACCESS.2021.3114030

Disturbance and Uncertainty Rejection-Based on Fixed-Time Sliding-Mode Control for the Secure Communication of Chaotic Systems

VAN NAM GIAP[1], HONG SON VU[2], QUANG DICH NGUYEN[3], AND SHYH-CHOUR HUANG[1], (Senior Member, IEEE)

[1]Department of Mechanical Engineering, National Kaohsiung University of Science and Technology, Kaohsiung 807618, Taiwan
[2]Faculty of Electronics and Electrical Engineering, Hung Yen University of Technology and Education, Hung Yen 160000, Vietnam
[3]Institute for Control Engineering and Automation, Hanoi University of Science and Technology, Hai Ba Trung, Hanoi 100000, Vietnam

Corresponding authors: Hong Son Vu (hongson.ute@gmail.com) and Shyh-Chour Huang (shuang@nkust.edu.tw)

This work was supported by the Ministry of Science and Technology, Republic of China, under Contract MOST 110-2221-E-992-062.

ABSTRACT This study provides a new development regarding uncertainty and disturbance estimation (UDE) based on fixed-time sliding mode control (FTSMC) for the secure communication of electronic circuits in a chaos-based system. Takagi-Sugeno (T-S) fuzzy systems were used to remodel chaotic systems with the aim of softening the control design for the synchronization of the chaos-based system. The master and slave systems of the secure communication system were maintained in chaotic formats. The originality of the proposed uncertainty and disturbance estimator is a condition associated with the first derivative of these values being free. The stability of the system was proven by using the Lyapunov condition. The states of master and slave systems were used for encryption and decryption, respectively. Finally, the correction of the proposed control theories was verified by MATLAB simulations, the simulation of the electronic circuits in OrCAD capture software, and experiments involving electronic circuit communication.

INDEX TERMS Disturbance and uncertainty estimation, Takagi-Sugeno fuzzy system, secure communication, fixed-time sliding mode control.

I. INTRODUCTION

Disturbance observers are well-known as robust control techniques for the suppression of perturbations from outside and inside of a control system. There is no exception for a secure communication system (SCS). A disturbance to an SCS may be passed from the input channels or through variations in system parameters. Since secure communication based on chaotic systems first appeared, many practical papers have dealt with the problem of synchronization control design and disturbance and uncertainty compensation. Chen *et al.* [1] proposed a secure communication structure based on computer communication. In [2], the secure communication of two nonidentical logic circuits was archived with the support of a sliding-mode control (SMC) method. The paper ignored that, when a circuit is implemented in an experiment, changes in the mainboard uncertainties, capacitors, and resistors always occur. Therefore, a disturbance observer for tolerance control techniques is highly recommended. Our paper [3] proposed the synchronization of two chaotic systems based on linear matrix inequality and a time-varying disturbance observer. That paper stopped at the synchronization stage. In [4], a secure communication system with the synthesis of an adaptive disturbance observer (DOB) and SMC for chaos-based secure communication was proposed. The correction of the proposed control method was verified by an experiment involving computer and electronic circuit communication. The synchronization of the chaotic system based on the electronic circuits was applied in a radar application [5]. The chaos synchronization application in satellite secure communication was found in [6]. An application of chaotic systems in image security can be found in [7]–[10]. Implementations of secure communications based on circuits systems were presented in [11]–[15]. The synchronization of a network system was reported in [16]–[20]. The concept of synchronization was used for stable nonlinear bilateral teleportation manipulators with the support of adaptive fuzzy backstepping control [21]. The synchronization concept was

The associate editor coordinating the review of this manuscript and approving it for publication was Shen Yin.

also considered in [22], wherein a radial basic function neural network was designed to estimate the parameter variation in a multilateral telerobotic system. To suppress the disturbance and uncertainty of synchronization is a complicated task, and the MSSs are in chaotic formats. This approach will decrease the difficulty of perturbation estimator design if the mathematical portions of these master and slave systems can be changed into the formats of T-S fuzzy systems. However, the originality characteristic of the synchronization system is still maintained if the T-S fuzzy model is used to build a control algorithm while the master and slave systems have chaotic formats. Notably, the number of control designs for the secure communication of the T-S fuzzy chaos-based system is limited. This paper uses the master and slave in secure communication in chaotic formats. Control design based on T-S fuzzy systems is used to feed to the control input channels. After all, the power of the proposed method is maintained by precisely synchronizing the states of master and slave systems (MSSs).

The T-S fuzzy system was found in 1985 [23]. The representation of T-S fuzzy system modeling methods was investigated by Tanaka and Wang in [24]. The concepts of sector nonlinearity was briefly introduced. The T-S fuzzy model consists of fuzzy membership functions and sublinear systems. The design of control and synchronization for T-S fuzzy systems was investigated in [25]–[28]. To the best of our knowledge, the number of investigations of disturbance observer-based control for T-S fuzzy systems and the synchronization of chaos-based T-S fuzzy systems are limited. This paper uses the Chen model from [29]. The states of the original Chen system are out of the range of $[-15; 15]$. To apply the mathematical mode of the Chen chaotic system in an electronic circuit is challenging. To solve this problem, the system states needs to be rescaled. The details of the rescaled system procedure are given later. The rescaled system need to meet the characteristics of the original system. To obtain the price synchronization of the chaos-based system, the disturbances and uncertainty must be completely deleted.

The disturbance observer is well-known as an unknown input observer that uses the output signal and control input to construct compensated perturbations. The perturbations from both inside and outside the system strongly affect the desired outcomes and directly influence the performance of the control system. This paper uses the basic concept of the nonlinear disturbance observer (NDOB) in [30] to construct a new DOB. The developments of the basic NDOB was investigated in [31]–[33]. The perturbation observers require the assumption that the first derivative disturbance is equal to zero. To soften this assumption, this paper proposes a new disturbance observer to delete the perturbations from both sides of the secure communication system without the condition of the first derivative of perturbations. To correctly obtain disturbance values, the precision of the control system is a very important factor. Here, fixed-time sliding-mode control was proposed for synchronizing the MSS.

SMC is well-known as a nonlinear control technique, and it consists of equivalent control and switching control. These control values are used to stabilize the system states on a sliding surface and force state convergences on a predefined surface [34]. In [35], a new stochastic sliding mode surface was introduced as the chattering of the sliding mode control appearing from the switching control gain and the boundary layer thickness of the switching function [36]. In [4], an adaptive law with the integration of tracking error values was used to update the switching control gain. Fuzzy logic control was used to regulate the fixed sliding mode surface boundary and reduce the chattering value for an active magnetic bearing system [37]. An adaptive boundary layer SMC was proposed in [38]. Chattering can be reduced with a suitable switching control gain [39]. The SMC in this paper includes a fixed-time control strategy for the reaching phase and a finite-time strategy for the sliding phase. All the DOB and SMC components are used for the secure communication of chaotic systems. Secure communication operation is based on the synchronization of the states of MSSs. A sent signal is encrypted by the state of the master system, and a mixed signal is transferred to a public line. A mixed signal can be decrypted by the slave system state. The precision of the recovery data depends on the precision of synchronization control.

Some motivations from previous published papers are as follows: In [2], an SMC was used to synchronize the master and slave of a logical element chaotic system, and the synchronization outcome was good under ideal conditions. However, the synchronization overshoot and settling times were still high. Additionally, the disturbance and uncertainty problem was not considered. In our paper [3], the disturbance observer was still complicated. In [4], the first-derivative disturbance value was removed under the conditions of sliding-mode control. These limited problems are solved in a simple way in this paper. Furthermore, in [40], the synchronization system was proposed based on feedback control. However, disturbance suppression was ignored. Motivated by previous papers, this paper proses a new DOB to solve the problem of perturbation effects for a synchronization system. Furthermore the fixed-time concept may not be found in electronic circuits. The special consideration of this paper is the implementation of a fixed-time strategy by using electronic circuits, which will be introduced from an experimental study. The calculations of signum functions, and exponential functions can be represented in electronic circuits. The main contributions and novelties of this study are briefly introduced as follows:

1. In this study, the scale of the Chen system was reduced to fulfill the request of the electronic circuit voltage ranges. Then, the chaotic format was converted into the format of a T-S fuzzy system by using the sector nonlinearity method. The converted system was used as the control design implementation. The MSSs are maintained in the form of chaotic systems. This contribution is a suggestion for the applications of a recalled chaotic system in the

secure communication design and in the chaos control theory field.

2. The effects of perturbations from outside and inside of a secure communication system were softened by a new disturbance observer to obtain the precision synchronization goal. The disturbance observer in this paper is developed based on the DOB in a previously published study [30]. However, the problem of first derivative disturbance value conjunction is solved completely. The contribution of the solving problem of the boundary of the first derivative disturbance will open a direction for the application of the improved DOB method in other control systems. The proposed disturbance observer in this paper is first present for the basic nonlinear systems before it is implemented in a real synchronization system. This effort provides an overview of the application of the proposed DOB for nonlinear systems.
3. To synchronize the MSS, a fixed-time sliding-mode control was introduced in the secure communication system. Herein, the fixed-time concept is newly implemented in electronic circuits. This is a new suggestion for fixed-time control-based hardware implementation. The originality of the proposed fixed-time function is represented by the simple function of $sign(s^{\delta})$, which is simpler and effective in both a small and big initial state. This contribution is aimed to give a direction to the optimal fixed-time control method for the micro movement control system.
4. To verify that the proposed control theories are effective for secure communication in chaos-based systems in implementation and theory, the Lyapunov condition was chosen to solve the stability problem. All the theories were verified by MATLAB simulations, OrCAD Capture simulations, and experimental studies of electronic circuits.

Note that the T-S fuzzy model was used for control design so that the method used to enhance the synchronization of the chaos-based system could easily access the perturbations from both outside and inside the system. The organization of this work is as follows: The proposed control, related synchronization, and secure communication techniques are introduced in the first section. Second, the mathematics of the master and slave systems are introduced in modeling with T-S formats. In addition, the preliminaries of the finite and fixed time operations are briefly introduced. Third, the proposed disturbance observer and the synchronization control are introduced in detail in section III. Fourth, the illustrative examples are given in MATLAB simulation, OrCAD Capture software simulation, and experimental study to verify that the proposed theories are correct and real. Final, the conclusion and some comments for our future work are given in the last section.

Notations: $I^{m\times m}$ is identity matrix. A^T is transposition of A. If $s = [\,s_1,\ s_2, \ldots, s_n\,]^T$ and $s \in R^n$ then $sign(s) = sign[\,s_1,\ s_2, \ldots, s_n\,]^T$, and the exponent of the sign function is calculated as $sign(s^{\delta}) = s^{\delta}/\,|s|^{\delta} = sign^{\delta}(s)$.

II. MATHEMATICAL MODELING, SYNCHRONIZATION PROBLEMS DESCRIPTION, AND PRELIMINARY MATHEMATICS

This section presents the mathematical modeling of MSS into the formats of T-S fuzzy systems, the synchronization problem formulations, and the basic concept of the fixed-time sliding mode control and disturbance observer. The origination of this section is as follows: (A) the mathematical modeling of MSS and synchronization problem are presented, and (B) some mathematical preliminaries are given.

A. MATHEMATICAL MODELING AND SYNCHRONIZATION PROBLEM

This study used the Chen system in [29] to construct the MSS. Basically, the magnitude of the system states is used to determine that the system can or cannot be implemented on the electronic circuits. The system with full disturbance and uncertainty values is rewritten as follows:

$$\begin{cases} \dot{x}_1(t) = -(a+\Delta a)x_1(t) + (a+\Delta a)x_2(t) + d_{x_1}(t) \\ \dot{x}_2(t) = -(\tau+\Delta a)x_1(t) + (c+\Delta c)x_2(t) \\ \qquad\qquad - x_1(t)x_2(t) + d_{x_2}(t) \\ \dot{x}_3(t) = x_1(t)x_2(t) - (b+\Delta b)x_2(t) + d_{x_3}(t) \end{cases} \tag{1}$$

where $x_1(t), x_2(t)$ and $x_3(t)$, are system states. The system parameters in [29] were chosen as $a = 35$, $b = 3$, $c = 28$, and $\tau = a - c$, Δa, Δb, Δc, and $\Delta\tau$ are the system parameters variation values of a, b, c, and τ respectively. $d_{x_1}(t)$, $d_{x_2}(t)$, and $d_{x_3}(t)$ are the disturbance on the $x-$, $y-$ and $z-$axis, respectively. The performances of system (1) were chaos, unpredictable, nonperiodic. Furthermore, the system states are out of the range $[-15, 15]$. To apply the concept and phenomenon of the Chen system (1) to the electronic circuits, the scales of the system states need to be the subsets of the range $[-15, 15]$. The rescale process is taken as $x(t) \rightarrow x_1(t)/10$, $y(t) \rightarrow x_2(t)/10$, and $z(t) \rightarrow x_3(t)/20$ respectively. System (1) can work as its original phenomenon if the assumption below is satisfied.

Assumption 1: The system (1) is reliable if the disturbance on each axis and the parameter variations are all bounded as follows $|\Delta a| \le a_1, |\Delta\tau| \le \tau_1, |\Delta c| \le c_1, |\Delta b| \le b_1$, $\left|d_{x_1}(t)\right| \le d_1, \left|d_{x_2}(t)\right| \le d_2$, and $\left|d_{x_3}(t)\right| \le d_3$, respectively, where $a_1, \tau_1, b_1, c_1, d_1, d_2$, and d_3 are all positively defined.

Combining assumption 1 and the rescale process, system (1) is now remodeled as follows:

$$\begin{cases} \dot{x}(t) = -(a+\Delta a)x(t) + (a+\Delta a)y(t) + d_x(t) \\ \dot{y}(t) = (-\tau+\Delta\tau)x(t) + (c+\Delta c)y(t) \\ \qquad\qquad -20x(t)z(t) + d_y(t) \\ \dot{z}(t) = 5x(t)y(t) - (b+\Delta b)z(t) + d_z(t) \end{cases} \tag{2}$$

where disturbance on the $x-$, $y-$, and $z-$axes is referred to as $d_x(t)$, $d_y(t)$, and $d_z(t)$, respectively.

Remark 1: The disturbance and uncertainty on the $x-$, $y-$, and $z-$axes of the system (2) all need to be bounded as assumption 1.

System (2) is now converted to the other format as

$$\begin{bmatrix}\dot{x}(t)\\ \dot{y}(t)\\ \dot{z}(t)\end{bmatrix} = \begin{bmatrix}-a & a & 0\\ -\tau & c & -20x(t)\\ 0 & 5x(t) & -b\end{bmatrix}\begin{bmatrix}x(t)\\ y(t)\\ z(t)\end{bmatrix} + \begin{bmatrix}-\Delta a & \Delta a & 0\\ -\Delta\tau & \Delta c & 0\\ 0 & 0 & -\Delta b\end{bmatrix}\begin{bmatrix}x(t)\\ y(t)\\ z(t)\end{bmatrix} + \begin{bmatrix}1 & 0 & 0\\ 0 & 1 & 0\\ 0 & 0 & 1\end{bmatrix}\begin{bmatrix}d_x(t)\\ d_y(t)\\ d_z(t)\end{bmatrix} \tag{3}$$

System 2 is completely nonlinear. Constructing the disturbance observer for system (3) is still difficult. To convert system (3) to the T-S fuzzy system, the system as follows

$$\begin{cases}\dot{\zeta}(t) = h^m(\zeta(t), \\ \qquad u(t))\zeta(t) + g^m(\zeta(t), u(t))u(t) + Dd(t)\\ \delta(t) = l^m(\zeta(t), \\ \qquad u(t))\zeta(t)\end{cases} \tag{4}$$

should be considered, where $\zeta(t)$ is the system state vector and $\delta(t)$ is the system output vector. h^m, g^m, and l^m are smoothing functions. $u(t)$ is a control input vector and $d(t)$ is a disturbance value. The state of the system needs to be a subset of a fixed range as $\zeta_i(t) \in [\zeta_{\min}(t); \zeta_{\max}(t)]$. The fuzzy variable schedules are now calculated as follows:

$$\begin{cases} n_0^j(.) = \dfrac{\zeta_{j\max} - \zeta_j(.)}{\zeta_{j\max} - \zeta_{j\min}}\\ n_1^j(.) = 1 - n_0^j(.)\end{cases} \tag{5}$$

The fuzzy membership function is $\omega(\zeta_i)(t)$, with:

$$\phi_i(\zeta_j)(t) = \prod_{j=1}^{p} \phi_{ij}(\zeta_j)(t) \tag{6}$$

where $\phi_i(\zeta_{ij})(t) = n_0^j$ or $n_1^j(.)$. Applying the sector nonlinearity to system (4) yields:

$$\begin{cases}\dot{\zeta}(t) = \sum_{i=1}^{r} \phi_i(\zeta_j(t))[(A_i + \Delta A_i)\zeta(t)\\ \qquad + (B_i + \Delta B_i)u(t) + D_i d(t)]\\ \delta(t) = C\zeta(t)\end{cases} \tag{7}$$

where $\zeta(t) \in R^{n\times m}$ is the state; $u(t) \in R^{p\times m}$ is the control, and $\delta(t) \in R^{q\times m}$ is the system output vectors, respectively. $d(t) \in R^{k\times m}$ is the disturbance. $A_i \in R^{n\times n}, B_i \in R^{n\times p}$, and $C \in R^{q\times n}$ are approximated matrices. $\Delta A_i \in R^{n\times n}$ and $\Delta B_i \in R^{n\times p}$ are uncertainty matrices $D_i \in R^{n\times k}$ is the approximated matrix of disturbance.

Remark 2: To easily design the controller and observer for the T-S fuzzy system as in Eq. (7), the approximated matrices B_i and D_i should be chosen as the identity matrices.

Assumption 2: System (7) can work as its original characteristics, and the lumped perturbations need to be bounded by $|D_i d(t)| < \overline{d}, |\Delta A_i| \le \overline{a}, |\Delta B_i| \le \overline{b}$, respectively, where $\overline{d}, \overline{a}$, and $\overline{b}$ are all positively defined.

Assumption 3: To simplify the calculation process, the disturbance and uncertainty are assumed to be calculated as one unique term as $\Delta A_i x(t) + \Delta B_i u(t) + D_i d(t) = E_i\gamma(t)$. The perturbation is defined by $\gamma(t) = [\,\gamma_1(t),\ \gamma_2(t),\ \gamma_3(t)\,]^T$.

Remark 3: To easily obtain the information of perturbations, the approximated matrix E_i is strongly recommended to be identity.

System (7) can be simplified as:

$$\begin{cases}\dot{\zeta}(t) = \sum_{i=1}^{r} \phi_i(\zeta_j(t))\{A_i\zeta(t) + B_i u(t) + E_i l(t)\}\\ \delta(t) = C\zeta(t)\end{cases} \tag{8}$$

Using the sector nonlinearity of the T-S fuzzy modeling, system (2) is remodeled into the format as follows:

$$\dot{\zeta}(t) = \sum_{i=1}^{2} \phi_i(\zeta_i(t))[A_i X(t) + B_i u(t) + E_i l(t)] \tag{9}$$

where

$$\zeta = [\,x \quad y \quad z\,]^T, \quad \phi_1(x(t)) = (5 + x(t))/10,$$
$$\phi_2(x(t)) = (5 - x(t))/10, \quad A_1 = \begin{bmatrix}-a & a & 0\\ -\tau & c & -100\\ 0 & 25 & -3\end{bmatrix},$$
$$A_2 = \begin{bmatrix}-a & a & 0\\ -\tau & c & 100\\ 0 & -25 & -3\end{bmatrix},$$
$$E_1 = E_2 = \begin{bmatrix}1 & 0 & 0\\ 0 & 1 & 0\\ 0 & 0 & 1\end{bmatrix},$$

and $B_1 = B_2 = \begin{bmatrix}1&0&0\\0&1&0\\0&0&1\end{bmatrix}$. With parameters and initial values as $\zeta(0) = [\,0.1\ 0.05\ -0.05\,]^T$, $u(t) = [\,0\ 0\ 0\,]^T$ and $d(t) = [\,0\ 0\ 0\,]^T$, system states and the phase trajectories are shown in Figure 1 below.

These system states in Figure 1 above show that the rescaled system is chaotic and nonperiodic. The states are now ranged into the spaces of the subset of $[-15, 15]$. The conversion of the Chen system from the format of a chaotic system into the format of a T-S fuzzy system involves no loss of system characteristics. The phase portraits of the rescaled system are used to confirm that the rescaled T-S fuzzy system is correct according to the original system (1). System phase trajectories are shown in Figure 2.

Taking the advantage of the Chen system, the master states of the secure communication are modelled as follows:

$$\begin{cases}\dot{x}_m(t) = -(a + \Delta a_m)x_m(t) + (a + \Delta a_m)y_m(t)\\ \dot{y}_m(t) = (-\tau + \Delta\tau_m - 20z_m(t))x_m(t)\\ \qquad + (c + \Delta c_m)y_m(t)\\ \dot{z}_m(t) = 5x_m(t)y_m(t) - (b + \Delta b_m)z_m(t)\end{cases} \tag{10}$$

where $x_m(t)$, $y_m(t)$, and $z_m(t)$ are states of the master system. The system parameter are maintained as $a = 35, b = 3$,

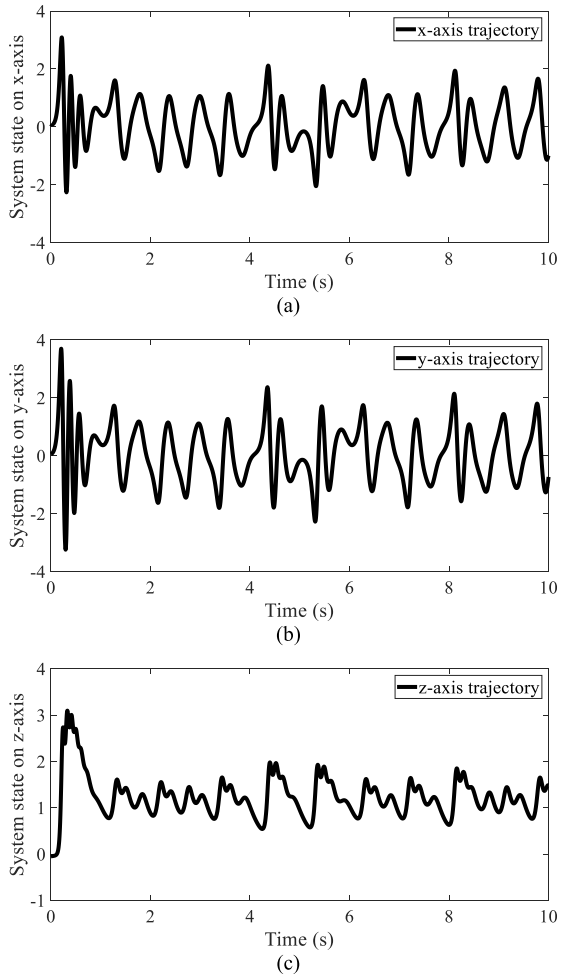

FIGURE 1. System states: (a) state on x-axis, (b) state on y-axis, and (c) state on z-axis.

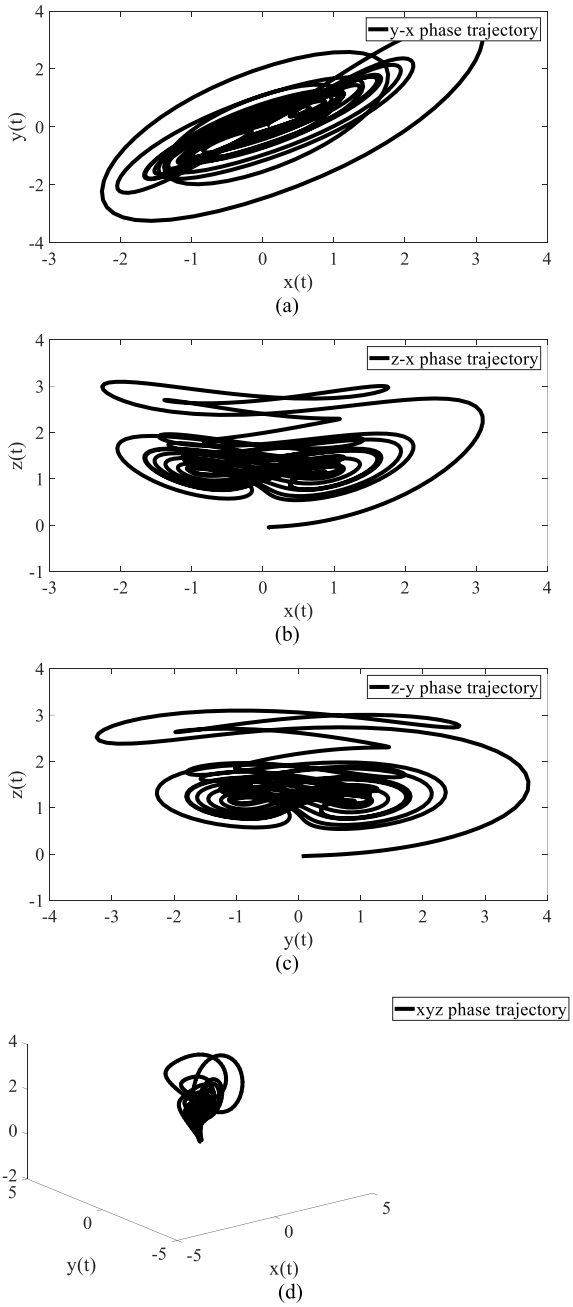

FIGURE 2. Phase trajectories: (a) yx-trajectory, (b) zx-trajectory, (c) zy-trajectory, and (d) xyz-trajectory.

$c = 28$, and $\tau = a - c.\Delta a_m, \Delta b_m, \Delta c_m$, and $\Delta\tau_m$ are the system parameters variation values of a, b, c, and τ, respectively.

Assumption 4: The system (10) can work with its own characteristics if the disturbance on each axis and the parameter variations are all bounded as follows: $|\Delta a x_m(t)| \leq a_{1m}, |\Delta a y_m(t)| \leq a_{2m}, |\Delta\tau x_m(t)| \leq \tau_{1m}, |\Delta c y_m(t)| \leq c_{1m}, |\Delta b z_m(t)| \leq b_{1m}$, respectively. Where $a_{1m}, a_{2m}, c_{1m}, \tau_{1m}$, and b_{1m} are all positively defined.

The slave system mathematical modeling with the control inputs is presented as follows:

$$\begin{cases} \dot{x}_s(t) = -(a + \Delta a_s)x_s(t) + (a + \Delta a_s)y_s(t) \\ \qquad + u_{xs}(t) + d_{xs}(t) \\ \dot{y}_s(t) = (-\tau + \Delta\tau_s - 20z_s(t))x_s(t) + (c + \Delta c_s)y_s(t) \\ \qquad + u_{xs}(t) + d_{ys}(t) \\ \dot{z}_s(t) = 5x_s(t)y_s(t) - (b + \Delta b_s)z_s(t) + + u_{xs}(t) + d_{zs}(t) \end{cases} \quad (11)$$

where $x_s(t), y_s(t)$, and $z_s(t)$ are states of the master system. $u_{xs}(t), u_{ys}(t)$, and $u_{zs}(t)$ are the control inputs on the $x-$, $y-$, and $z-$axes, respectively. The system parameters are maintained as $a = 35, b = 3, c = 28$, and $\tau = a - c.\Delta a_s, \Delta b_s, \Delta c_s$, and $\Delta\tau_s$ are the system parameters variation values of a, b, c, and τ, respectively. $d_{xs}(t), d_{ys}(t), d_{zs}(t)$ are the disturbance on the x_s-, y_s-, and z_s-axes, respectively.

Assumption 5: The system (11) can work as its own characteristics if the disturbance on each axis and the parameter variations are all bounded as follows: $|\Delta a x_s(t)| \leq a_{1s}, |\Delta a y_s(t)| \leq a_{2s}, |d_{xs}(t)| \leq d_{1s}, |\Delta\tau x_s(t)| \leq \tau_1 s, |\Delta c y_s(t)| \leq c_{1s}, |d_{ys}(t)| \leq d_{2s}, |\Delta b z_s(t)| \leq b_{1s}, |d_{zs}(t)| \leq d_{3s}$, respectively, where $a_{1s}, a_{2s}, d_{1s}, c_{1s}, d_{2s}, b_1 s, d_3 s$ are all positively defined.

Basically, the secure communication for the data transmission can be guaranteed by the support of the chaotic system state.

Remark 4: The accuracy of T-S fuzzy modeling depends on the antecedent variables for the sector nonlinearity modeling method and the number of the linearization points for the linearization method, respectively. The antecedent variables and linearization points are all experimentally chosen by the designer.

The operation of the secure communication in this paper is as follows:

$$\hat{S}(t) = y_m(t) + S(t) - y_s(t) \tag{12}$$

where $S(t)$ is the secret signal that needs to be securely transferred form master area to slave area. $\hat{S}(t)$ is the received signal. To obtain the precise secure signal in the slave area, the master and slave system states precisely track each other as $y_m(t) = y_s(t)$. This paper used the T-S fuzzy model to construct the controller and observer. The MSSs are then maintained in the form of the chaotic systems. The models of master and slave systems are temporarily transferred to the format of the T-S fuzzy systems as follows:

$$\begin{cases} \dot{\zeta}_m(t) = \sum_{i=1}^{2} \phi_i(x_m(t))[A_i\zeta_m(t) + E_i l_m(t)] \\ \dot{\zeta}_s(t) = \sum_{i=1}^{2} \phi_i(x_s(t))[A_i\zeta_s(t) + B_i u_s(t) + E_i l_s(t)] \end{cases} \tag{13}$$

where m and s are used to represent the master and slave notations, respectively. The control input appears on the slave side. The tracking errors are described as follows:

$$e(t) = \zeta_m(t) - \zeta_s(t) \tag{14}$$

Taking the derivative of both sides of Eq. (14) yields:

$$\dot{e}(t) = \sum_{i=1}^{2} \phi_i(x_m(t))[A_i\zeta_m(t) + E_i l_m(t)] - \sum_{i=1}^{2} \phi_i(xs(t))[A_i\zeta_s(t) + B_i u(t) + E_i l_s(t)] \tag{15}$$

Due to $\sum_{i=1}^{2} \phi_i(x_m(t)) = 1$ and $\sum_{i=1}^{2} \phi_i(x_s(t)) = 1$, the disturbance and uncertainty of the synchronization system can be calculated as a unique term. The calculation is represented as follows:

$$\dot{e}(t) = \sum_{i=1}^{2} \phi_i(x_m(t))[A_i\zeta_m(t)] - \sum_{i=1}^{2} \phi_i(x_s(t))[A_i\zeta_s(t) + B_i u(t)] + E_i(l_m(t) - l_s(t)] \tag{16}$$

As shown in remarks 2 and 3, the approximated matrices are chosen as $B_i = I_{3\times3}$ and $E_i = I_{3\times3}$. By referring $\bar{l} = l_m(t) - l_s(t)$, the derivative tracking error equation (15) can be calculated as a new model as follows:

$$\dot{e}(t) = \sum_{i=1}^{2} \phi_i(x_m(t))[A_i\zeta_m(t)] - \sum_{i=1}^{2} \phi_i(x_s(t))[A_i\zeta_s(t)] - B_i u(t) + E_i\bar{l} \tag{17}$$

This paper uses fixed-time sliding-mode control for synchronizing the master and slave systems. To soften the effects of disturbance and uncertainty, a new disturbance observer is proposed for the synchronization system.

Remark 5: To obtain the precision tracking of master and slave systems, the states on $x-$, $y-$, and $z-$axes of these system need to precisely track each other. The precision of tracking control is dependent on the synchronization control algorithm.

The preliminaries of mathematical operations are given in the next following section below.

B. PRELIMINARY MATHEMATICAL CALCULATIONS

This section presents some preliminary mathematical calculations of fine and fixed-time stability. The beginning concepts for the system are as follows:

$$\dot{x}(t) = f(t, x) \tag{18}$$

Definition 1 ([41]): Finite-time stability concept where $x \in R^P$ is the state vector. System (18) is called finite-time stable if the origin is Lyapunov stable and exists in an open neighborhood $D \in R^P$, and positive $T(x(0))$ is the settling time with:

$$\begin{cases} \lim_{t\to T(x_0)} x(t) \to 0 \\ x(x_0) = 0 \end{cases} \tag{19}$$

Theorem 1: System as follows:

$$s = -\kappa sign(s) \tag{20}$$

consists of a finite-time stable as

$$T_s < T_{\max} = \frac{|s(0)|}{\kappa} \tag{21}$$

Proof: Lyapunov candidate should be selected as follows:

$$V(t) = \frac{1}{2}s^2(t) \tag{22}$$

Taking derivative for both sides of Eq. (22) have

$$\dot{V}(t) = s(t)\dot{s}(t) \tag{23}$$

or

$$\begin{aligned} \dot{V}(t) &= -\kappa s(t) sign(s(t)) \\ &= -\kappa\,|s(t)| \\ &= -\kappa V^{0.5}(t) \end{aligned} \tag{24}$$

Taking integration for both sides of Eq. (24) corresponding to the time from zero to settling time $T_{\max}$ yields

$$\int_{V(0)}^{V(T_{\max})} \frac{dV(t)}{V^{1/2}(t)} = -\int_{V(0)}^{V(T_{\max})} \kappa dt \tag{25}$$

or

$$2V^{\frac{1}{2}}(T_{\max}) - 2V^{\frac{1}{2}}(0) = -\kappa T_{\max} \tag{26}$$

or

$$T_{\max} = \frac{|s(0)|}{\kappa} \tag{27}$$

Remark 6: The stability of finite-time was introduced to the synchronization control system to look for the finite-time sliding phase.

This complete proof of Theorem 1.

Definition 2 ([42]) Fixed-Time Stability Concept:

If the system (18) is globally finite-time stable and the settling time is limited by a constant value, as follows:

$$\begin{cases} T(x(0)) < T_{\max} \\ T_{\max} > 0, \end{cases} \quad \forall \zeta(0) \tag{28}$$

System (18) is then called fixed-time stable.

Theorem 2: The equation

$$\dot{s}(t) = -\gamma_1 |s(t)|^{\frac{a_1}{b_1}} sign(s(t)) - \gamma_2 |s(t)|^{\frac{a_2}{b_2}} sign(s(t)) \tag{29}$$

Have fixed time stability $T_{\max} = \frac{1}{\gamma_2}\frac{b_2}{b_2-a_2} + \frac{1}{\gamma_1}\frac{b_1}{(a_1-b_1)}$.

Proof: The Lyapunov candidate can be chosen with one dimension as follows:

$$V(s(t)) = \frac{1}{2}s^2(t) \tag{30}$$

Ignoring the time (t) for softening the writing and taking the derivative of both sides of Eq. (30) yields

$$\begin{aligned} \dot{V}(s) &= s\dot{s} \\ &= s[-\gamma_1 |s|^{\frac{a_1}{b_1}} sign(s) - \gamma_2 |s|^{\frac{a_2}{b_2}} sign(s)] \\ &= -\gamma_1 s^{2\frac{a_1+b_1}{2b_1}} - \gamma_2 s^{2\frac{a_2+b_2}{2b_2}} \\ &= -\gamma_1 V(s)^{\frac{a_1+b_1}{2b_1}} - \gamma_2 V(s)^{\frac{a_2+b_2}{2b_2}} \\ &= [-\gamma_1 V(s)^{\frac{a_1+b_1}{2b_1} - \frac{a_2+b_2}{2b_2}} - \gamma_2] V(s)^{\frac{a_2+b_2}{2b_2}} \le 0 \end{aligned} \tag{31}$$

If $\dot{V}(s) \le 0$ system (18) is globally bounded. When $V(\delta) \neq 0$ have

$$\frac{1}{V(s)^{\frac{a_2+b_2}{2b_2}}}\frac{dV(s)}{dt} = -\gamma_1 V(s)^{\frac{a1+b_1}{2b_1} - \frac{a_2+b_2}{2b_2}} - \gamma_2 \tag{32}$$

or

$$\frac{1}{V(s)^{\frac{a_2+b_2}{2b_2}}}\frac{dV(s)}{dt} = -\gamma_1 V(s)^{\frac{a1+b_1}{2b_1} - \frac{a_2+b_2}{2b_2}} - \gamma_2$$

$$\frac{1}{\gamma_1 V(s)^{\frac{b_2a_1-b_1a_2}{2b_1b_2}} + \gamma_2}\frac{dV(s)^{\frac{b_2-a_2}{2b_2}}}{dt} = \frac{b_2-a_2}{b_2} \tag{33}$$

Integrating (33) over the time from zero to T yields

$$\int_{V(s(0))}^{V(s(\infty))} \frac{dV(s(t))^{\frac{b_2-a_2}{2b_2}}}{\gamma_1 V(s(t))^{\frac{b_2-a_2}{2b_2}[\frac{(b_2a_1-b_1b_2)}{b_1(b_2-a_2)}+1]} + \gamma_2} = \frac{b_2-a_2}{2b_2}T_{\max} \tag{34}$$

or

$$\begin{aligned} T_{\max} &< \frac{1}{\frac{b_2-a_2}{b_2}}\int_{V(0)}^{V(1)}\frac{d\varsigma}{\gamma_2} \\ &\quad + \frac{1}{\frac{b_2-a_2}{b_2}}\int_{V(1)}^{V(\infty)}\frac{dV(s)^{\frac{b_2-a_2}{2b_2}}}{\gamma_1 V(s)^{\frac{(b_2a_1-b_1b_2)}{2b_1b_2}+\frac{b_2-a_2}{2b_2}}} \\ &= \frac{1}{\gamma_2}\frac{b_2}{b_2-a_2} + \frac{1}{\gamma_1}\frac{b_2}{b_2-a_2}\frac{b_1(b_2-a_2)}{(b_2a_1-b_1b_2)} \end{aligned} \tag{35}$$

or

$$T_{\max} = \frac{1}{\gamma_2}\frac{b_2}{b_2-a_2} + \frac{1}{\gamma_1}\frac{b_1}{(a_1-b_1)} \tag{36}$$

This complete proof of Theorem 2.

Remark 7: The stability of fixed-time was used to look for reaching phase control.

All details of proposed control algorithms are shown in the next sections.

III. DISTURBANCE AND UNCERTAINTY REJECTION BASED ON FIXED-TIME SLIDING-MODE CONTROL FOR THE SECURE COMMUNICATION OF CHAOTIC SYSTEMS

To delete the disturbance and perturbations of system parameters variations, an improvement of DOB is constructed for the slave system via the control input channel. The illness of the previous disturbance observer in [30] was proven in our recent paper [4]. The first derivative disturbance observer can be softened by a new observer in this paper. Otherwise, to suppress these perturbations perfectly, the fixed-time sliding-mode control was designed for the synchronization system. These control methods took advantages to perform secure communication for data transmission. This section presents in detail the proposed control algorithms as follows:

A. DISTURBANCE OBSERVER FOR A SYNCHRONIZATION SYSTEM

The proposed disturbance observer of Chen [30] is reconsidered in this paper, and a significantly improved method is given to solve the problem of the first derivative disturbance conjunction. The mathematical model of the new disturbance observer is given for the general system as

$$\dot{x}(t) = ax(t) + bu(t) + cd(t) \tag{37}$$

where $x(t)$ is the system state vector; $u(t)$ is the control input vector, and $d(t)$ is the disturbance value. a, b, and c are the approximated matrices of the state, control input, and disturbance values, respectively. The DOB mathematical model is shown as:

$$\begin{cases} \dot{p}(t) = -L_d cp(t) - L_d[ax(t) + bu(t) + cq(t)] \\ q(t) = L_d x(t) \\ \hat{d}(t) = L^{-1}(\frac{\alpha}{Ts+1}) \cdot (p(t) + q(t)) \end{cases} \tag{38}$$

where L_d is observer gain. $L^{-1}(\cdot)$ is meant to be the inversed Laplace operation. $(\cdot)$ is the convolution operation.

Remark 8: In previous papers, [30]–[33] ignored the high frequency disturbance value. By using Eq. (38), the low and high frequencies of disturbance values are all rejected.

We have:

$$\hat{d}(s) = \frac{\alpha}{Ts+1}[p(s)+q(s)] \tag{39}$$

or

$$(Ts+1)\hat{d}(s) = \alpha[p(s)+q(s)] \tag{40}$$

Subtracting both sides of Eq. (40) by the disturbance in the Laplace domain leads to:

$$d(s) - (Ts+1)\hat{d}(s) = d(s) - \alpha[p(s)+q(s)] \tag{41}$$

or

$$\tilde{d}(s) - Ts\hat{d}(s) = d(s) - \alpha[p(s)+q(s)] \tag{42}$$

Substituting Eq. (39) into Eq. (42) yields:

$$\tilde{d}(s) - Ts\frac{\alpha}{Ts+1}[p(s)+q(s)] = d(s) - \alpha[p(s)+q(s)] \tag{43}$$

Eq. (43) can be simplified as:

$$\tilde{d}(s) + \frac{\alpha}{Ts+1}[p(s)+q(s)] = d(s) \tag{44}$$

or the disturbance error is described as follows:

$$\tilde{d}(s) = d(s) - \frac{\alpha}{Ts+1}[p(s)+q(s)] \tag{45}$$

Going back to the time domain representation of disturbance, the error is now modeled as follows:

$$\tilde{d}(t) = d(t) - L^{-1}\left(\frac{\alpha}{Ts+1}\right)\cdot[p(t)+q(t)] \tag{46}$$

The disturbance error goes to zero if

$$\hat{d}(t) = L^{-1}\left(\frac{\alpha}{Ts+1}\right)\cdot[p(t)+q(t)] \tag{47}$$

At this point, the disturbance observer error goes to zero if the term of $\hat{d}(t)$ is compensated by the control channel as in Eq. (38). The details of the sliding mode control are provided in the following section, below. By applying the concept of the improved disturbance observer to the synchronization system, the DOB of the synchronization system is:

$$\begin{cases} \dot{p}_i(t) = -L_d E p_i(t) - L_{di}[\sum_{i=1}^{2}\phi_i(x_m(t))[A_i\zeta_{mi}(t)] \\ \qquad\qquad - \sum_{i=1}^{2}\phi_i(x_s(t))[A_i\zeta_s(t)] - B_i u(t) + E_i q_i(t)] \\ q_i(t) = L_{di}e_i(t) \\ \hat{\bar{l}}_i(t) = L^{-1}\left(\frac{\alpha_i}{T_i s+1}\right)\cdot(p_i(t)+q_i(t)) \end{cases} \tag{48}$$

where $i = 1 \div 3$ is the number of disturbance input channels on the $x-$, $y-$, and $z-$axes, respectively.

By using Eq. (48), we have:

$$\begin{aligned} \dot{p}_i(t) + \dot{q}_i(t) = & -L_d E p_i(t) - L_{di}[\sum_{i=1}^{2}\phi_i(x_m(t))A_i\zeta_{mi}(t) \\ & - \sum_{i=1}^{2}\phi_i(x_s(t))A_i\zeta_s(t) - B_i u(t) + E_i q_i(t)] \\ & + L_{di}\dot{e}_i(t) \end{aligned} \tag{49}$$

Combining Equations (17) and (49) yields:

$$\begin{aligned} \dot{p}_i(t) + \dot{q}_i(t) = & -L_{di}E_i p_i(t) - L_{di}[\sum_{i=1}^{2}\phi_i(x_m(t))A_i\zeta_{mi}(t) \\ & - \sum_{i=1}^{2}\phi_i(x_s(t))A_i\zeta_s(t) - B_i u(t) + E_i q_i(t)] \\ & + L_{di}[\sum_{i=1}^{2}\phi_i(x_m(t))A_i\zeta_{mi}(t) \\ & - \sum_{i=1}^{2}\phi_i(x_s(t))A_i\zeta_{si}(t) - B_i u(t) + E_i\bar{l}_i] \\ = & L_{di}E_i\bar{l} - L_{di}E_i(p_i(t)+q_i(t)) \\ = & L_{di}E_i[\bar{l}_i - (p_i(t)+q_i(t))] \end{aligned} \tag{50}$$

Taking the Laplace transform for the disturbance observer equation of Eq. (50) leads to:

$$\hat{\bar{l}}_i(s) = \frac{\alpha_i}{T_i s+1}(p_i(s)+q_i(s)) \tag{51}$$

Solving Eq. (51) yields:

$$(T_i s+1)\hat{\bar{l}}_i(s) = \alpha_i(p_i(s)+q_i(s)) \tag{52}$$

Using the Laplace transform of the disturbance to subtract both sides of Eq. (52) yields:

$$\bar{l}_i(s) - (T_i s+1)\hat{\bar{l}}_i(s) = \bar{l}_i(s) - \alpha_i(p_i(s)+q_i(s)) \tag{53}$$

or

$$\bar{l}_i(s) - \hat{\bar{l}}_i(s) = T_i s\hat{\bar{l}}_i(s) + \bar{l}_i(s) - \alpha_i(p_i(s)+q_i(s)) \tag{54}$$

By referring $\tilde{\bar{l}}_i(s) = \bar{l}_i(s) - \hat{\bar{l}}_i(s)$, Eq. (54) can be simplified as follows:

$$\tilde{\bar{l}}_i(s) = T_i s\hat{\bar{l}}_i(s) + \bar{l}_i(s) - \alpha_i(p_i(s)+q_i(s)) \tag{55}$$

Substituting Eq. (51) into Eq. (54) leads to:

$$\begin{aligned} \tilde{\bar{l}}_i(s) = & T_i s\frac{\alpha_i}{T_i s+1}(p_i(s)+q_i(s)) + \bar{l}_i(s) - \alpha_i(p_i(s)+q_i(s)) \\ = & (T_i s+1-1)\frac{\alpha_i}{T_i s+1}(p_i(s)+q_i(s)) + \bar{l}_i(s) \\ & - \alpha_i(p_i(s)+q_i(s)) \\ = & -\frac{\alpha_i}{T_i s+1}(p_i(s)+q_i(s)) + \bar{l}_i(s) \end{aligned} \tag{56}$$

Combining Equations (51) and (56), if the estimated is selected as Eq. (50), the disturbance tracking error value in Eq. (56) is equal to zero.

Remark 9: The development of the basic nonlinear disturbance observer with the support of the low-pass-filter suppresses all the low and high frequency disturbances to zero.

B. FIXED-TIME SLIDING-MODE CONTROL BASED ON THE DISTURBANCE OBSERVER FOR THE SYNCHRONIZATION SYSTEM

This paper used a fixed-time reaching phase and finite-time sliding phase to construct the sliding mode controller for a synchronization system. The sliding surface is selected as:

$$s(t) = e(t) + \lambda \int_0^t e(\tau) d\tau \tag{57}$$

Taking the derivative of both sides of Eq. (57) has:

$$\dot{s}(t) = \dot{e}(t) + \lambda e(t) \tag{58}$$

Solving Eq. (58) with $\dot{s}(t) = 0$ yields:

$$\dot{e}_j(t) = -\lambda_j e_j(t) \tag{59}$$

Taking integration for both sides of Eq. (59) corresponding to the time from zero to settling time $T_{\max}$ yields:

$$t_{j\max} = e^{-\lambda j t_{\max}} \tag{60}$$

The sliding phase is designated as follows:

$$\dot{s}_j(t) = -a_{1j} sign^{\frac{\alpha j}{\beta_{1j}}}(s_j(t)) - a_{2j} sign^{\frac{\alpha_{2j}}{\beta_{2j}}}(s_j(t)) \tag{61}$$

where $s(0) = s_0$ and $sign^k(s(t)) = sign(s(t)^k)$. If $a_{1j} > 0, a_{2j} > 0, \alpha_{1j}/\beta_{1j} > 1$, and $\alpha_{2j}/\beta_{2j} < 1$, by applying Theorem 2, the settling time is calculated as follows:

$$T_{si} < T_{i\max} = \frac{\alpha_{1i}}{a_{1i}(\alpha_{1i} - \beta_{1i})} + \frac{\beta_{1i}}{a_{2}i(\beta_{2i} - \alpha_{2i})} \tag{62}$$

where T_{sj} is settling time value of the sliding mode surface j^{th}. Applying the concept of the SMC to the synchronization system yields:

$$\dot{s}(t) = \sum_{i=1}^{2} \phi_i(x_m(t))[A_i \zeta_m(t)] - \sum_{i=1}^{2} \phi_i(x_s(t))[A_i \zeta_s(t)] + B_i u(t) + E_i(l_m(t) - l_s(t)] + \lambda e(t) \tag{63}$$

Solving Eq. (63) with the first derivative sliding surface is equal to zero with no disturbance value yields:

$$u_{eqj}(t) = [B_{i,j}^T B_{i,j}]^{-1} B_i^T [\sum_{i=1}^{2} \phi_i(x_m(t))[A_{i,j}\zeta_{mj}(t)] - \sum_{i=1}^{2} \phi_i(x_s(t))[A_{i,j}\zeta_{sj}(t)] + \lambda_{i,j} e_j(t)] \tag{64}$$

where $i = 1 \div 2$. $j = 1 \div 3$ is the number of the row of the matrix. The switching control is selected as follows:

$$u_{swj}(t) = [B_{i,j}^T B_{i,j}]^{-1} B_{i,j}^T [a_{1j} sign^{\frac{\alpha_{1j}}{\beta_{1j}}}(s_j(t)) + a_{2j} sign^{\frac{\alpha_{2j}}{\beta_{2j}}}(s_j(t))] \tag{65}$$

where

$$sign(s(t)) = \begin{cases} 1 & if\ s(t) > 0 \\ 0 & if\ s(t) = 0 \\ -1 & if\ s(t) < 0 \end{cases} \tag{66}$$

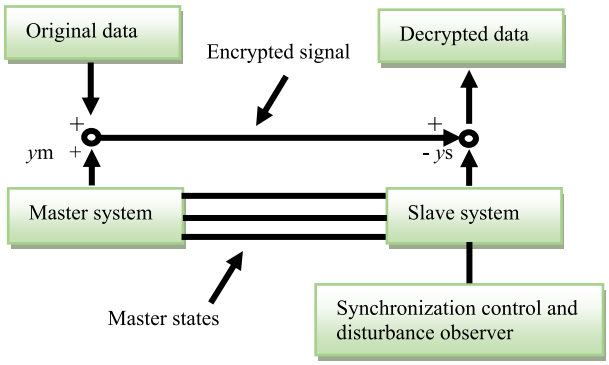

FIGURE 3. Secure communication system.

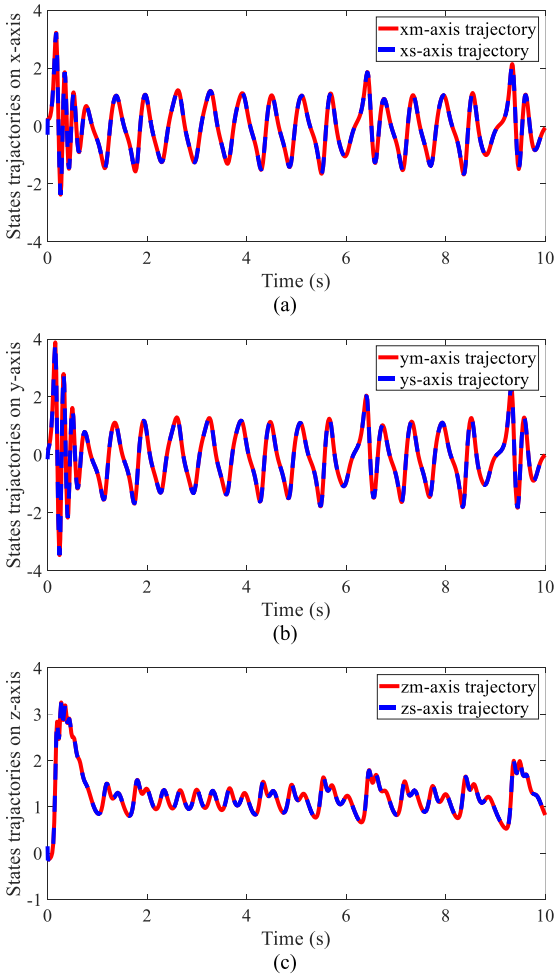

FIGURE 4. Synchronization signals: (a) xm(t) and xs(t), (b) ym(t) and ys(t), (c) zm(t) and zs(t).

The control values are shown in Equations (64) and (65) and the disturbance compensations are shown in Eq. (48). All proposed control algorithms are now applied to synchronize the chaotic system. The proposed control methods need to satisfy the convergence condition. This paper used the Lyapunov theorem to prove the stability of proposed algorithms. The details are shown in the following section.

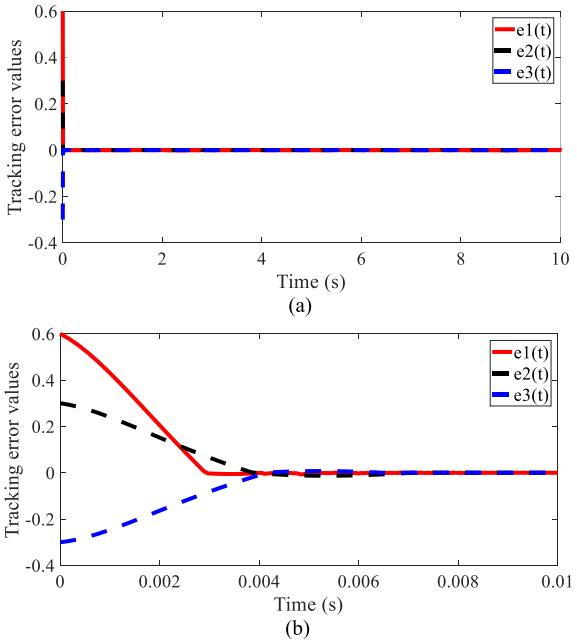

FIGURE 5. Synchronization errors: (a) the errors in the 10 seconds and (b) the errors in the first 0.01 second.

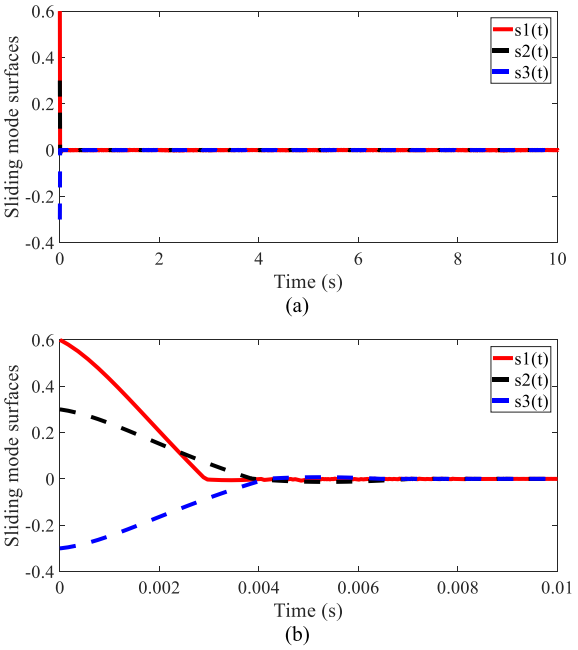

FIGURE 6. Synchronization sliding surfaces: (a) the surfaces in the first 10 seconds and (b) the surfaces in the first 0.1 second.

Remark 10: Take note that, if the disturbance and uncertainty can be completely suppressed, the switching control gains can be chosen as small values to reduce the chattering.

C. STABILITY ANALYSIS

The necessary condition is used to define the stability of the system with equivalent control value, which is used to satisfy the condition as:

$$\dot{e}(t) = \sum_{i=1}^{2} \phi_i(x_m(t))[A_i\zeta_m(t)] - \sum_{i=1}^{2} \phi_i(x_s(t))[A_i\zeta_s(t) + B_i u_{eq}(t)] + E_i\bar{l} \quad (67)$$

or

$$\begin{aligned}\dot{e}(t) = &\sum_{i=1}^{2} \phi_i(x_m(t))[A_i\zeta_m(t)] - \sum_{i=1}^{2} \phi_i(x_s(t))[A_i\zeta_s(t) \\ &+ B_i([B_i^T B_i]^{-1}B_i^T[\sum_{i=1}^{2} \phi_i(x_m(t))[A_i\zeta_m(t)] \\ &- \sum_{i=1}^{2} \phi_i(x_s(t))[A_i\zeta_s(t)] + \lambda e(t)])]+] \end{aligned} \quad (68)$$

or

$$\dot{e}(t) = -\lambda e(t) \quad (69)$$

The tracking error value goes to zero when the time goes to infinity if the λ is positively defined. The sufficient condition is selected as follows:

$$V_j(t) = \frac{1}{2}s_j^2(t) + \frac{1}{2}\tilde{d}_j^2(t) \quad (70)$$

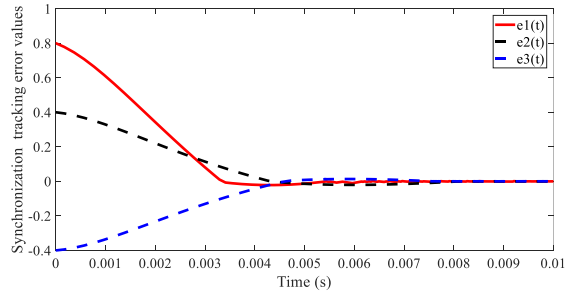

FIGURE 7. Synchronization errors in the first 0.01 second with $\zeta_m(0) = [0.4\ 0.2\ -0.2]$ and $\zeta_s(0) = -[0.4\ -0.2\ 0.2]$.

Taking derivative for both sides of Eq. (70) leads to

$$\begin{aligned}\dot{V}_j(t) &= s_j(t)\dot{s}_j(t) + \tilde{d}_j(t)\dot{\tilde{d}}_j(t) \\ &= s[-a_{1j}sign^{\frac{\alpha_{1j}}{\beta_{1j}}}(s(t)) - a_{2j}sign^{\frac{\alpha_{2j}}{\beta_{2j}}}(s(t))] + 0 \\ &\leq -a_{1j}\left|s_j(t)\right|^{\frac{\alpha_{1j}}{\beta_{1j}}+1} - a_{2j}\left|s_j(t)\right|^{\frac{\alpha_{2j}}{\beta_{2j}}+1} < 0 \end{aligned} \quad (71)$$

This completes the verification of the proposed method.

Remark 11: The settling of the control system is fixed-time. The poof of the fixed-time for Eq. (55) can be found in [43] when $s(t) > 1$ Eq. (55) is completely fulfilled. When $s(t) \ll 1$, the settling-time is limited by the bandwidth of $T_{j\max} < 1/(a_{1j} + a_{2j})$.

The correction of the proposed theories is verified by the simulation and experimental studies in the next sections.

IV. AN ILLUSTRATIVE EXAMPLE

This paper focuses on the theory of circuit analysis, which is used to verify that the finite and fixed time controls can

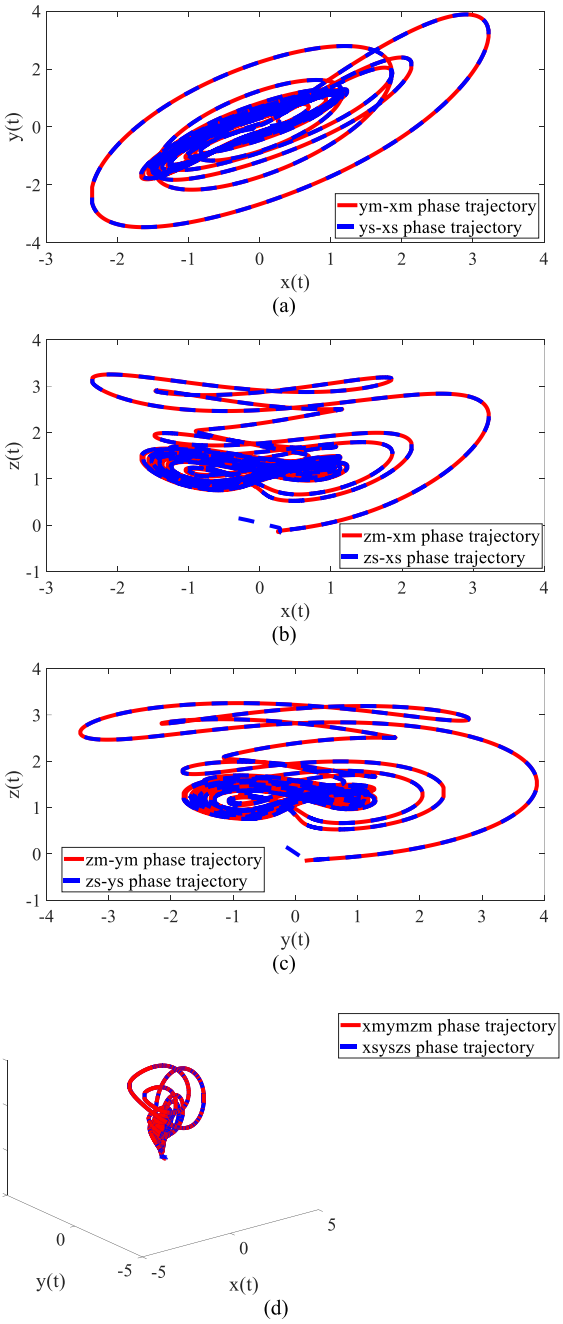

FIGURE 8. Synchronization phase trajectories of the master and slave systems: (a) the phase on x- and y-axes, (b) the phase on x- and z-axes, (c) the phase on y- and z-axes, and (d) the phase trajectories on x-, y-, and z-axes.

be implemented on a circuit. Due to the short distance of communication between master and slave circuit systems, the delay-time problem in the circuit was ignored. To achieve the desired goals, the simulation on MATLAB should be first given to verify that the effectiveness of the disturbance observer with all tested disturbance has been canceled by the proposed method. Furthermore, to illustrate the desired goal of electronic circuit implementation, simulation on Orcad Capture software is used to represent control synchronization

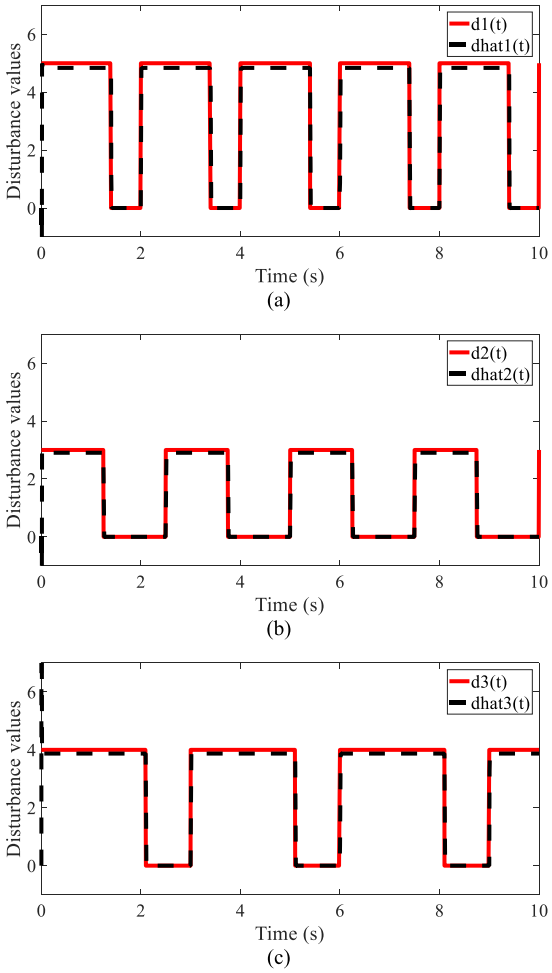

FIGURE 9. Tested and estimated disturbance values. (a) disturbances on x-axis, (b) disturbances on y-axis, and (c) disturbances on z-axis.

with application in secure communication. The secure communication system is shown as Figure 3 below.

All theories are verified as follows:

A. MATLAB SIMULATION PERFORMANCE

This section is briefly given to illustrate the effect of the proposed disturbance observer. The control parameters are selected as follows: $\lambda = \begin{bmatrix} 0.01 & 0 & 0 \\ 0 & 0.01 & 0 \\ 0 & 0 & 0.01 \end{bmatrix}$, $a_{11} = 50, a_{21} = 50, a_{12} = 10, a_{22} = 15, a_{13} = 10, a_{23} = 15, \alpha_{11} = 3, \beta_{11} = 4, \alpha_{21} = 7, \beta_{21} = 4, \alpha_{12} = 3, \beta_{12} = 5, \alpha_{22} = 5, \beta_{22} = 5, \alpha_{13} = 2, \beta_{13} = 4, \alpha_{23} = 3, \beta_{23} = 2, \alpha_1 = \alpha_2 = \alpha_3 = 30, L_d = \begin{bmatrix} 1 & 0 & 0 \\ 0 & 1 & 0 \\ 0 & 0 & 1 \end{bmatrix}$, and $T_1 = T_2 = T_3 = 0.001$. The initial conditions of MSS are $\zeta_m(0) = [0.3\ 0.15\ -0.15]$ and $\zeta_s(0) = [-0.3\ -0.15\ 0.15]$. The secure data are encrypted by a system state and transferred to the public channel. The encrypted data can be recovered

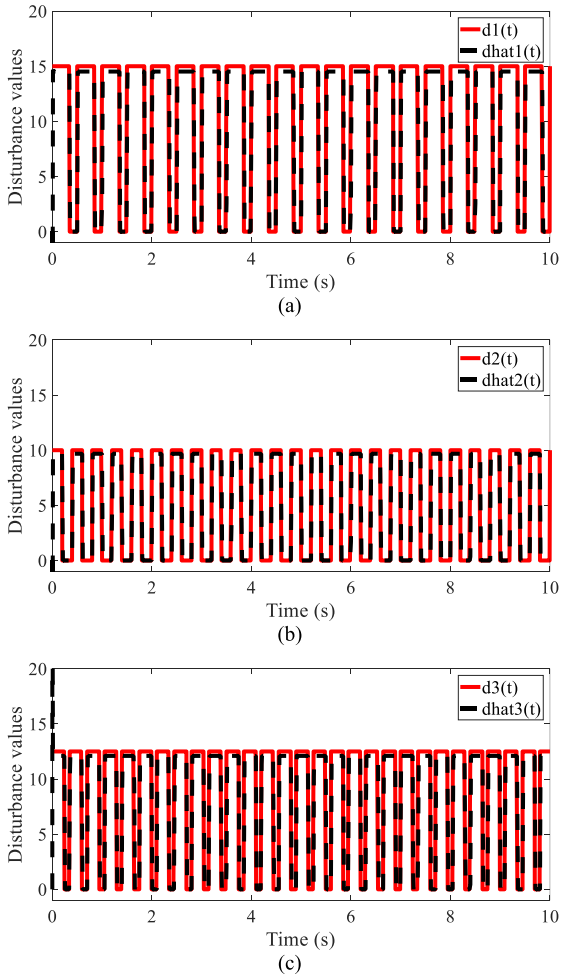

FIGURE 10. High frequency of the tested and estimated disturbance values. (a) Disturbances on x-axis, (b) disturbances on y-axis, and (c) disturbances on z-axis.

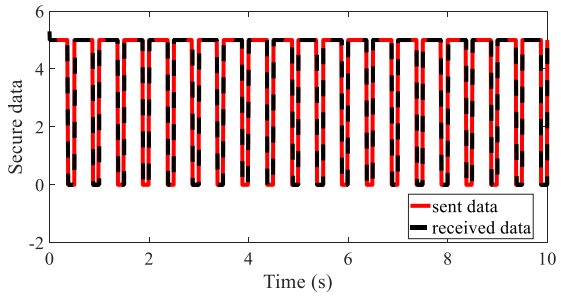

FIGURE 11. Sent and received signals.

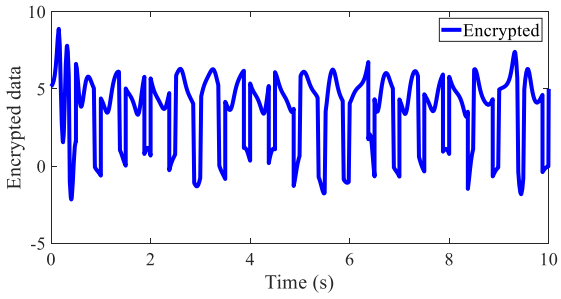

FIGURE 12. Encrypted data.

TABLE 1. A comparison of the proposed approach with paper [40].

Values	OUR RESULT	PAPER [40]
* *Maximum tracking error*	Maximum value is $1.25 \cdot 10^{-3}$	Smallest value is bigger than [-1; 1]
* *Maximum Steady-states*	$e1(t) \in [-1.25 \quad 1.1].10^{-3}$,	Bigger than 10^{-3}
* *Settling time*	Maximum value is 0.08 (second)	After 1 second
* *Background*	Simulation	Simulation

at the slave system area. The expectations of the secure transmission are the synchronization of the master and slave system so that the sent and received data are identical. The performances of the proposed control algorithms is shown in the Figures 4-12 below. First, the synchronization signals are shown in Figure 4 below.

Synchronization was precisely obtained, and the tracking error values on three axes are very small. The tracking error values are shown in Figure 5 below.

The settling times of the synchronization system on the $x-$, $y-$, and $z-$axes are $T_{e1} < 0.035$(s), $T_{e2} < 0.08$(s), and $T_{e3} < 0.08$, respectively. The tracking errors are in the range of $e_1(t) \in [-1.25 \ 1.1].10^{-3}$, $e_2(t) \in [-5.14 : 6.52].10^{-4}$, and $e_3(t) \in [-7.42 \ 8.74].10^{-4}$, for synchronization on $x-$, $y-$, and $z-$axes, respectively. The performance of sliding surfaces are shown in Figure 6, below.

The settling times for the sliding surface reaching the zero are mostly the same as the settling time of tracking errors. To inform the chaotic systems after synchronization and still maintain the original characteristics, the phase trajectories of the master and slave systems are shown in Figure 7 below. The performance of different initial condition is as follows:

With the same control parameters, the different initial conditions of MSSs as $\zeta_m(0) = [0.4 \ 0.2 \ -0.2]$ and $\zeta_s(0) = [-0.4 \ -0.2 \ 0.2]$ leads the reaching times of the tracking errors to be mostly same with it in case of $\zeta_m(0) = [0.3 \ 0.15 \ -0.15]$ and $\zeta_s(0) = [-0.3 \ -0.15 \ 0.15]$. The phase trajectories of MSSs with $\zeta_m(0) = [0.3 \ 0.15 \ -0.15]$ and $\zeta_s(0) = [-0.3 \ -0.15 \ 0.15]$ are in Figure 8 below.

As shown in the figures above, the proposed control methods are good at synchronizing master and slave chaotic systems. To verify the performance of the disturbance observer in Eq. (22), the tested disturbance is introduced directly to

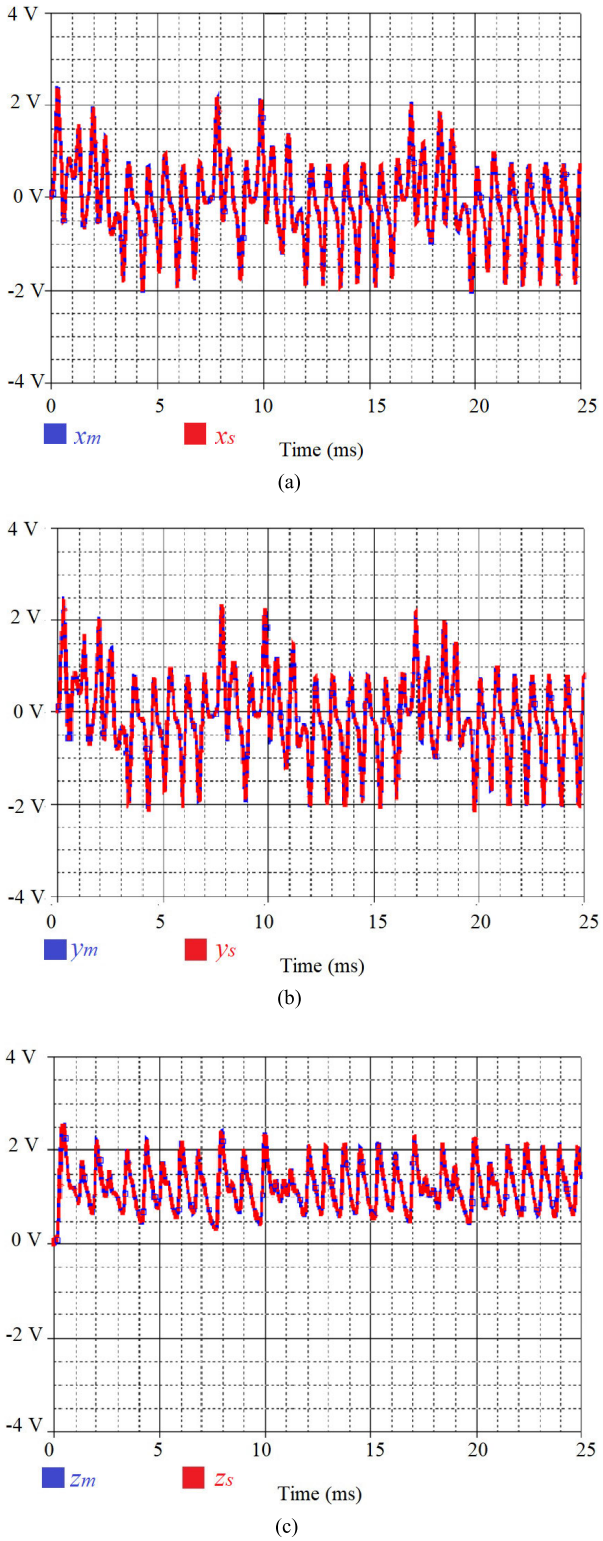

FIGURE 13. Synchronization states: (a) xm(t) and xs(t), (b) ym(t) and ys(t), and (c) zm(t) and zs(t).

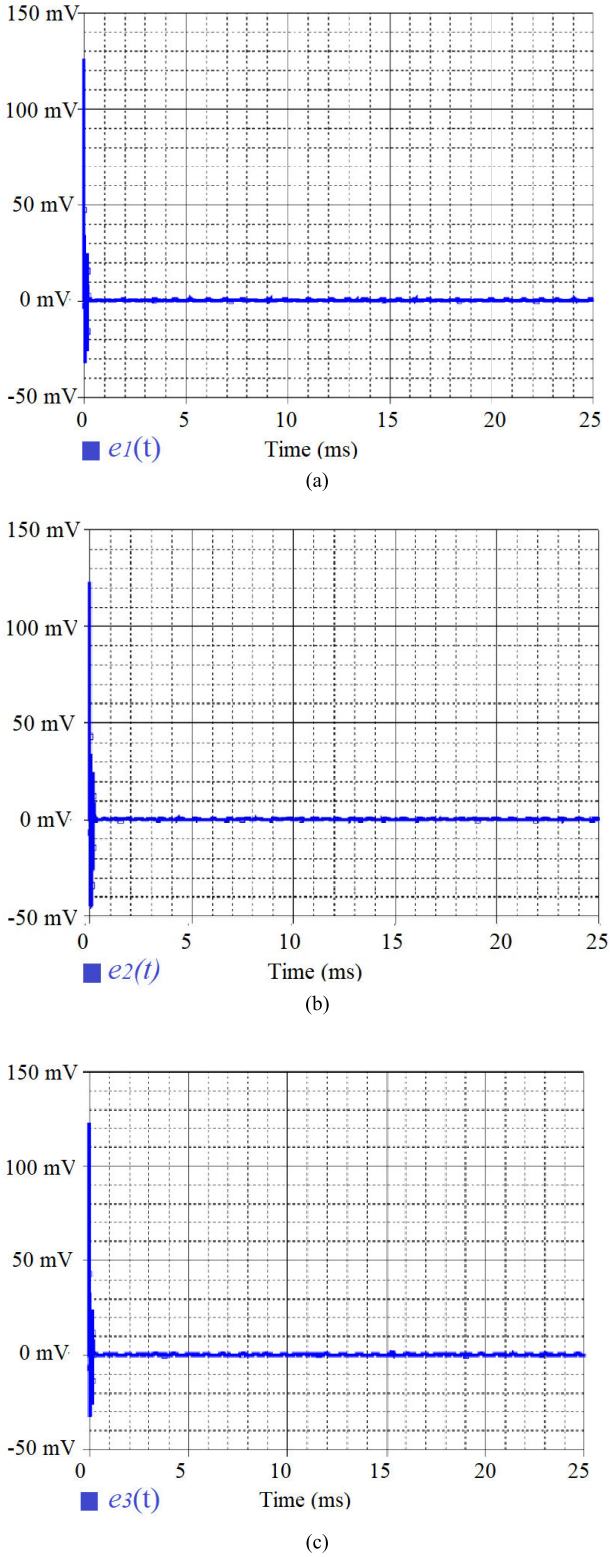

FIGURE 14. Synchronization tracking error values: (a) e1(t), (b) e2(t), and (c) e3(t).

the synchronization system via the control input channel. The performance of the proposed observer can be shown in Figure 9, below.

The tested disturbances were mostly covered by the estimated disturbance. Furthermore, the high magnitude and high frequency disturbances on three axes were tested on the

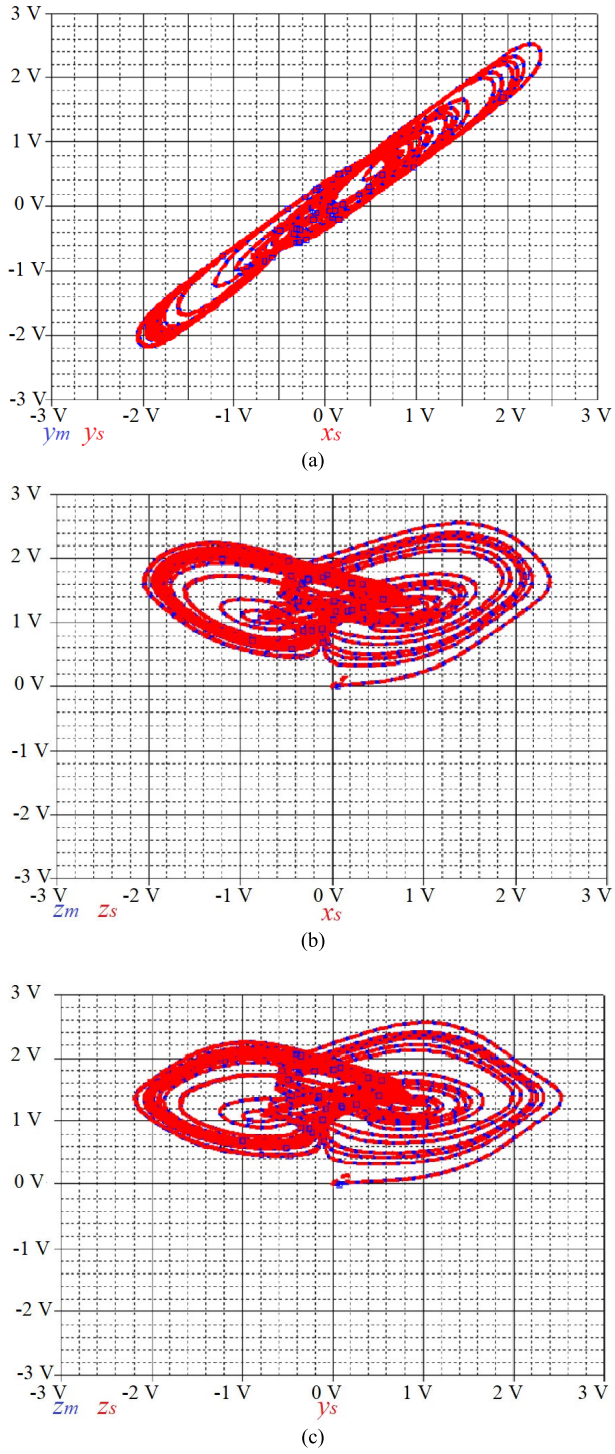

FIGURE 15. Synchronization phase portraits: (a) ym, ys and xm, (b) zm, zs and xm, and (c) zm, zs and ym.

system, and the performances of the disturbance observer with the same disturbance observer gains are shown in Figure 10 below.

Remark 12: The disturbance and uncertainty of the system were summed as a unique term on each axis. Therefore, the tested disturbances into the system are total perturbations.

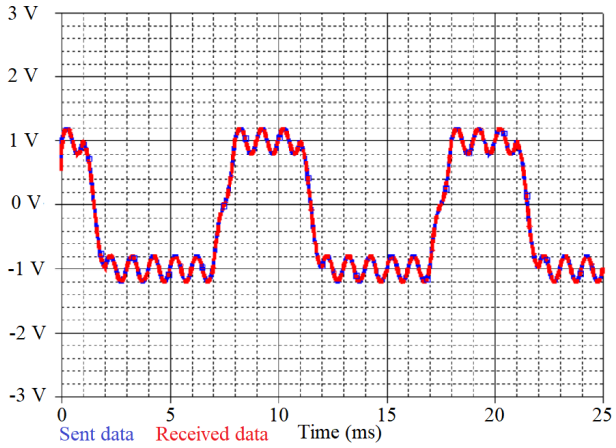

FIGURE 16. Sent and received signals.

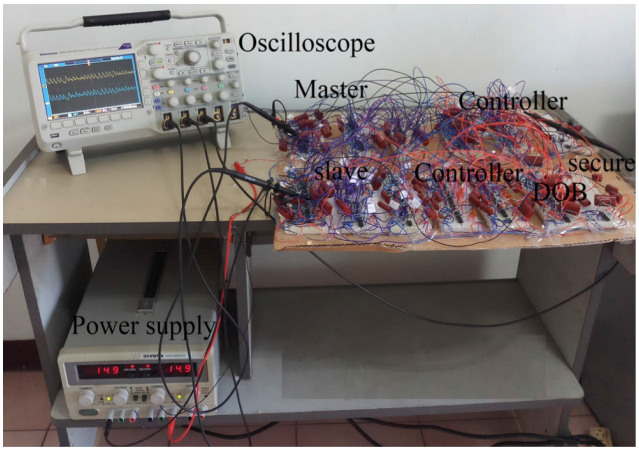

FIGURE 17. Experiment setup.

In the simulation, the disturbance was tested via input channels. In the experiment, the disturbance can be calculated by the proposed DOB.

The synchronization system takes advantage to do a secure transmission of the square wave signal. The sent and received signals are shown in Figure 11 below.

The encrypted signal is in Figure 12 below.

The effectiveness of the proposed control algorithms is compared to the previous published result in [40]. The comparison is shown as follows:

The control theories can be implemented on electronic circuits in the next section.

B. ORCAD CAPTURE SIMULATION PERFORMANCE

This section presents the simulation of the above control algorithms for electronic circuit design. The purpose of this section is to present the mathematical calculations of the finite- and fixed-time sliding-mode control for an electronic circuit. The operations for $sign(s_1^{0.75})$, and $sign(s_1^{1.25})$ are shown in the Appendix section. The control system parameters are selected as $a_{11} = 1, a_{21} = 1, a_{12} = 1,$

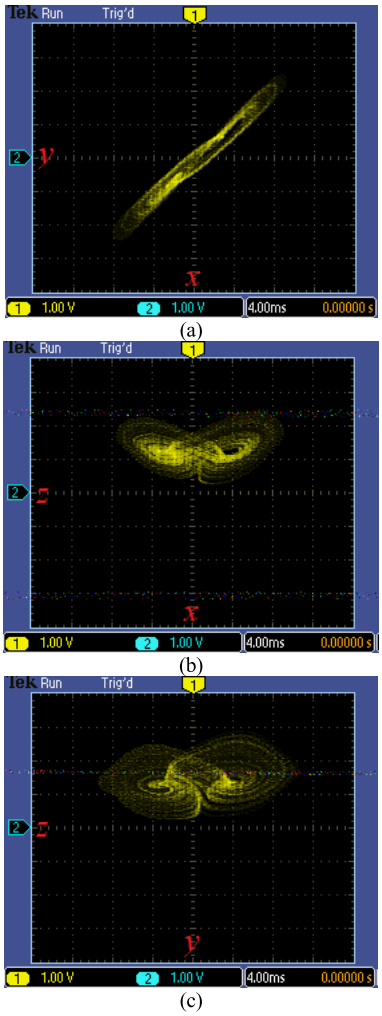

FIGURE 18. System phase portraits, (a) phase yx, (b) phase zx, and (c) phase zy.

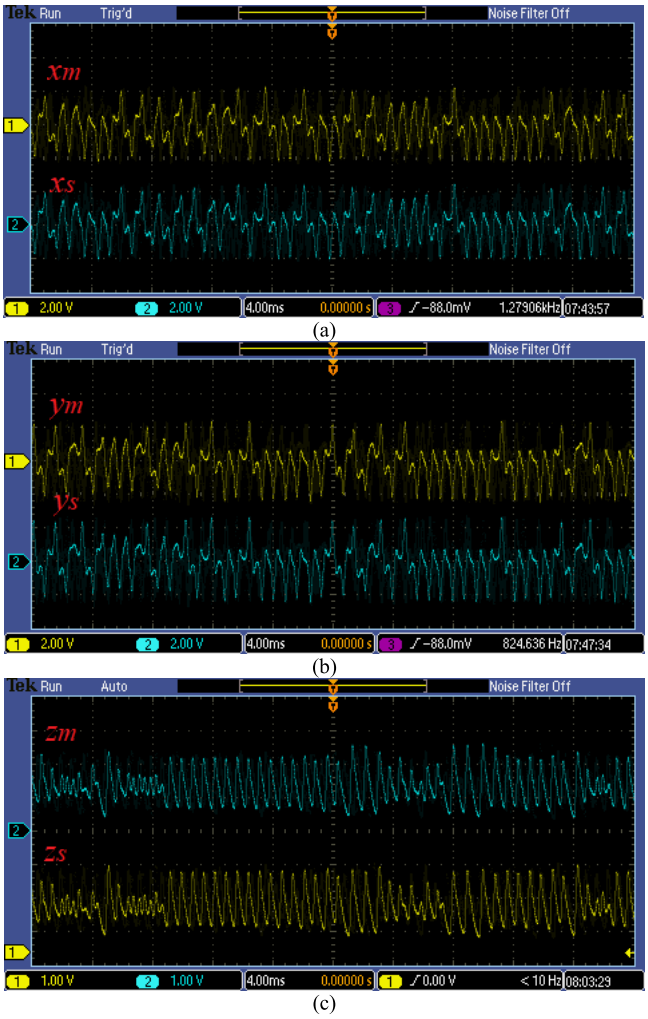

FIGURE 19. Synchronization signals, (a) xm and xs, (b) ym and ys, and (c) zm and zs.

$a_{22} = 1, a_{13} = 1, a_{23} = 1, \alpha_{11} = 3, \beta_{11} = 4, \alpha_{21} = 5, \beta_{21} = 4, \alpha_{12} = 3, \beta_{12} = 4, \alpha_{22} = 5, \beta_{22} = 4, \alpha_{13} = 3, \beta_{13} = 4, \alpha_{23} = 5, \beta_{23} = 4, \alpha_1 = \alpha_2 = \alpha_3 = 1, \lambda = \begin{bmatrix} 100 & 0 & 0 \\ 0 & 100 & 0 \\ 0 & 0 & 100 \end{bmatrix}, L_d = \begin{bmatrix} 250 & 0 & 0 \\ 0 & 250 & 0 \\ 0 & 0 & 400 \end{bmatrix}$, and $T_1 = T_2 = T_3 = 0.1$, and the initial conditions of the master and slave systems are determined by the capacitors and resistors of differential parts. All operations of the proposed method are shown in the Appendix. These above parameters were used to confirm that the proposed method can be applied to the electronic circuits. Furthermore, secure communication is implemented as shown in the Appendix section with different gains of DOB. The performance of the proposed algorithms are shown as Figures 13 to 16.

The master and slave systems mostly tracked with each other. The simulation was achieved under the ideal conditions so the tracking errors are very small, as shown in Figure 14 below.

The tracking error on the $x-$, $y-$, and $z-$axes are in the range of $e_1(t) \in (-40;\ 125)$ mV, $e_2(t) \in (-45;\ 122)$ mV, and $e_3(t) \in (-40;\ 122)$. The Orcad simulation can show the phase portrait for one pair of axes, with the minimal errors of the master and slave system states obtained, and the phase portrait can be seen in Figure 15 below.

Because the states of the master and slave systems are mostly identical, the phase trajectories of the slave system with the master state on the x-, y-, and z-axes are mostly stacked onside each other. The phase trajectories are used to verify that the master and slave systems after synchronization still maintain the chaotic forms. The outcome of the y-axis is used to decrypt the encrypted signal form the public channel. The signal is securely transmitted from the master to the slave system via the public channel with the support of the master state on the y-axis. The transmitted and received signals are shown in Figure 16 below.

Sent and received data are quite close to each other, which is again used to confirm that the proposed control algorithm is good at synchronizing two nonidentical chaotic systems.

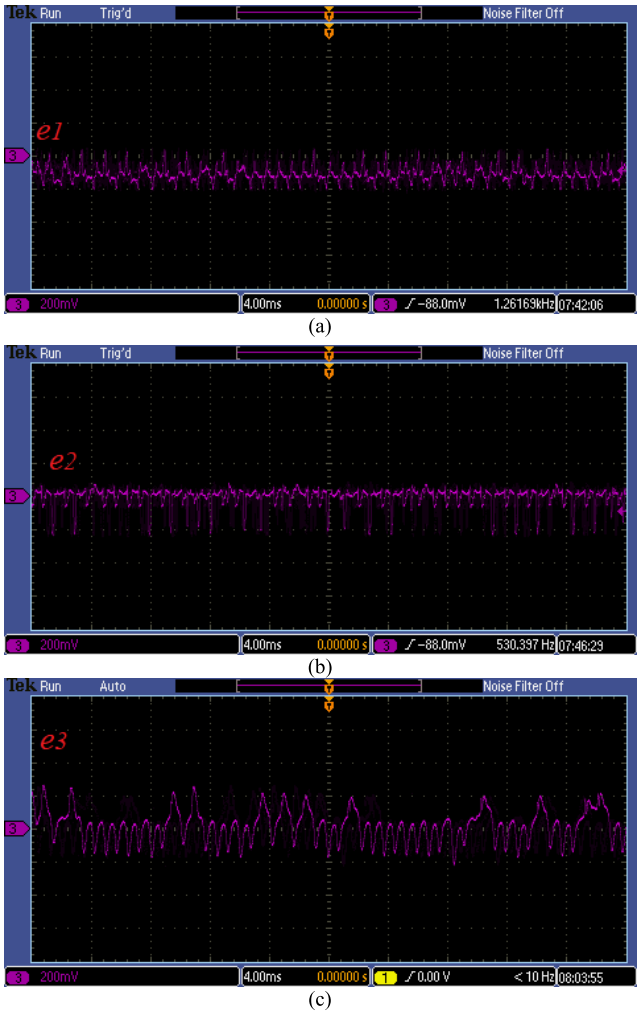

FIGURE 20. Synchronization errors, (a) e1, (b) e2, and (c) e3.

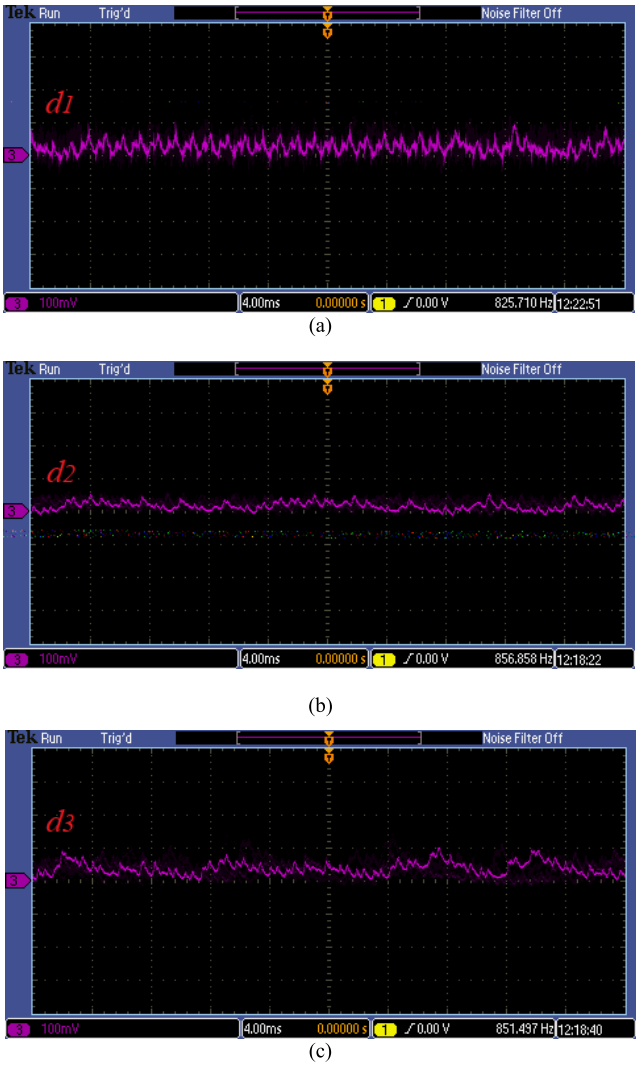

FIGURE 21. Perturbations in the circuit, (a) perturbation on x-axis, (b) perturbation on y-axis, and (c) perturbation on z-axis.

C. EXPERIMENT WITH PROPOSED METHODS ON ELECTRONIC CIRCUITS

This section presents the experimental results on the electronic circuit. The control parameters are the same as the simulation. The disturbance observer gain is $L_d = \begin{bmatrix} 100 & 0 & 0 \\ 0 & 100 & 0 \\ 0 & 0 & 100 \end{bmatrix}$. The experimental setup is in Figure 17 below.

The multiplications and division are achieved by the AD 633 JNZ, and the additions and subtractions were obtained by the AD 711 JNZ chips. System phase portraits are in Figure 18 below.

The synchronization of the chaos-based system with the support of the proposed theories is in Figure 19 below.

The states of the MSS on the x, y, and z-axes are mostly identical. These state errors are shown in the following Figure 20 below.

The tracking errors are $e_1(t) \in (-200;\ 20)$ mV, $e_2(t) \in (-220;\ 40)$ mV, and $e_3(t) \in (-200;\ 250)$ mV. These errors used to represent that the proposed methods are good for synchronization of the chaos-based system. The disturbance and uncertainty of the system can be estimated in Figure 21 below.

To show the effectiveness of the proposed theories, the data secure communication outcome is in Figure 22 below.

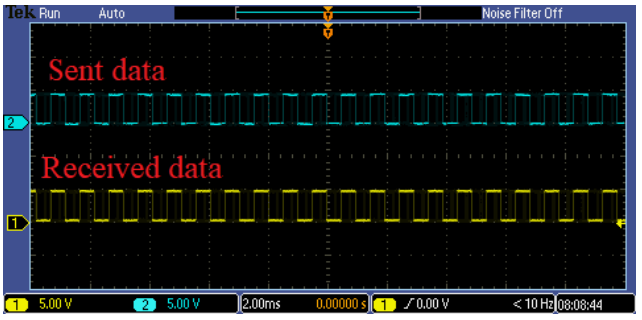

FIGURE 22. Secure communication data.

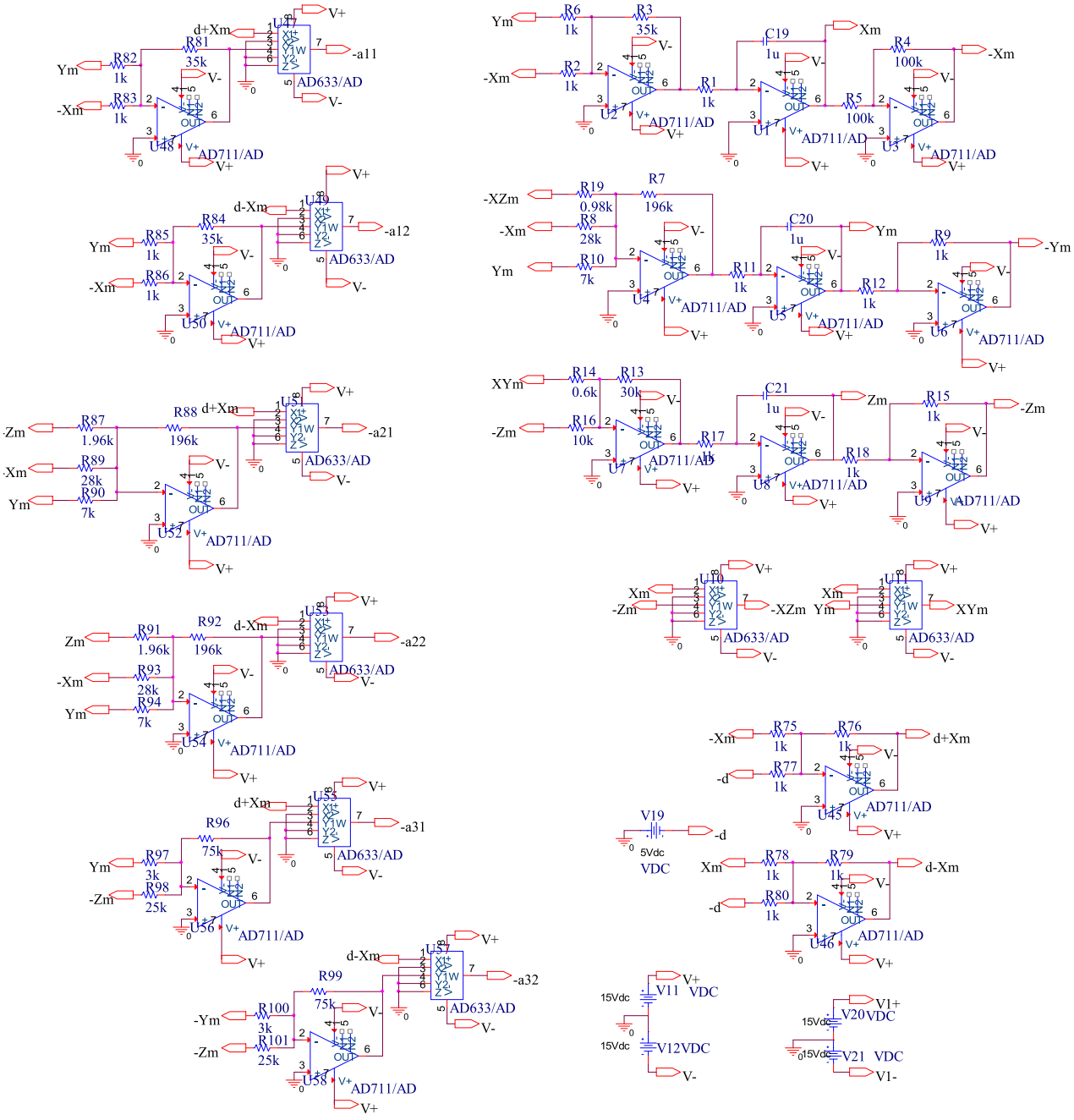

FIGURE 23. Master system and its T-S fuzzy model calculation.

In the secure communication system, the sent data were securely transferred from the master area to the slave area. The received and sent data are mostly identical. This performance once again suggested that the proposed methods are good regarding secure communication control.

V. CONCLUSION

This paper proposed a new disturbance observer to delete the perturbations of the secure communication system. The conjunction problem of the first derivative disturbance value was simply solved. To synchronize two different chaotic systems, such as a pair of master and slave systems, a fixed-time sliding mode was designed to meet the synchronization goals. A disturbance observer and sliding-mode control were built based on the format of the T-S fuzzy system for master and slave systems. The proposed control algorithms for a synchronization system provided security for a data communication system. The proposed theories were verified by simulations of two cases in the MATLAB and OrCAD

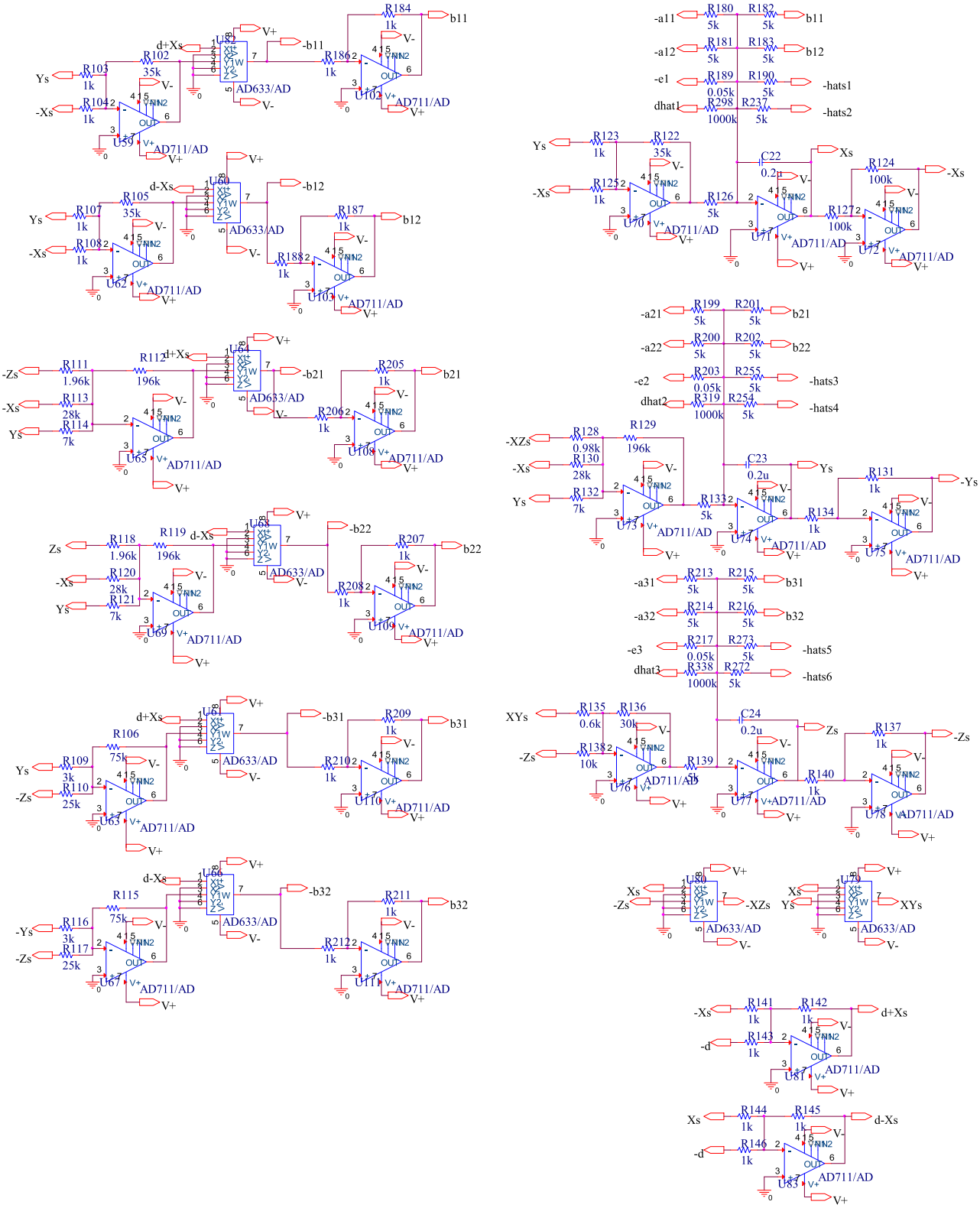

FIGURE 24. Slave system and its T-S fuzzy model calculation.

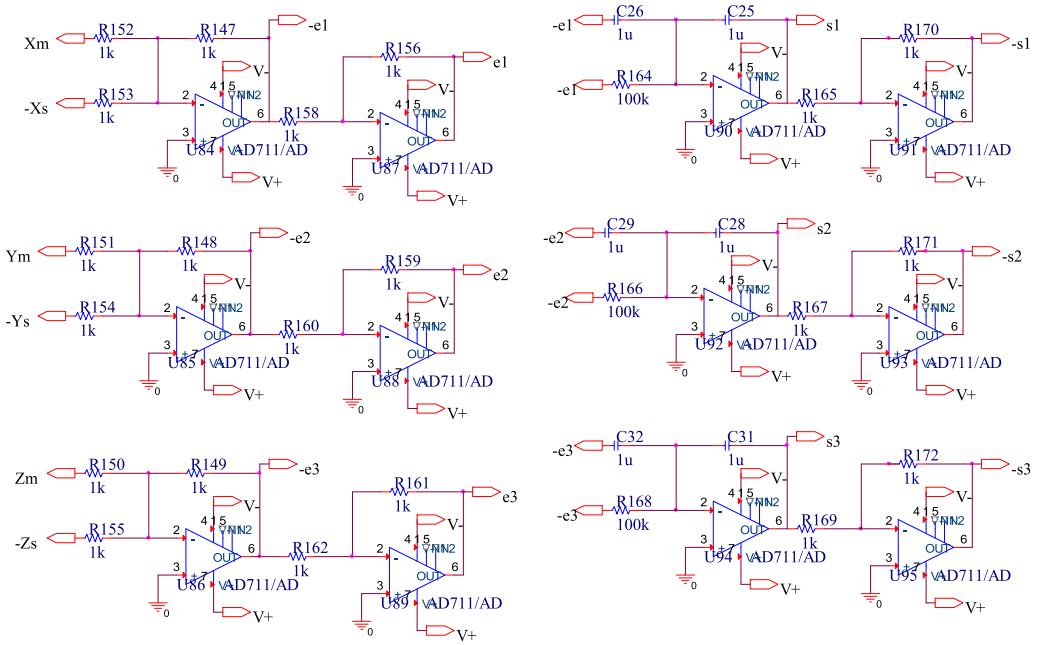

FIGURE 25. Synchronization tracking errors.

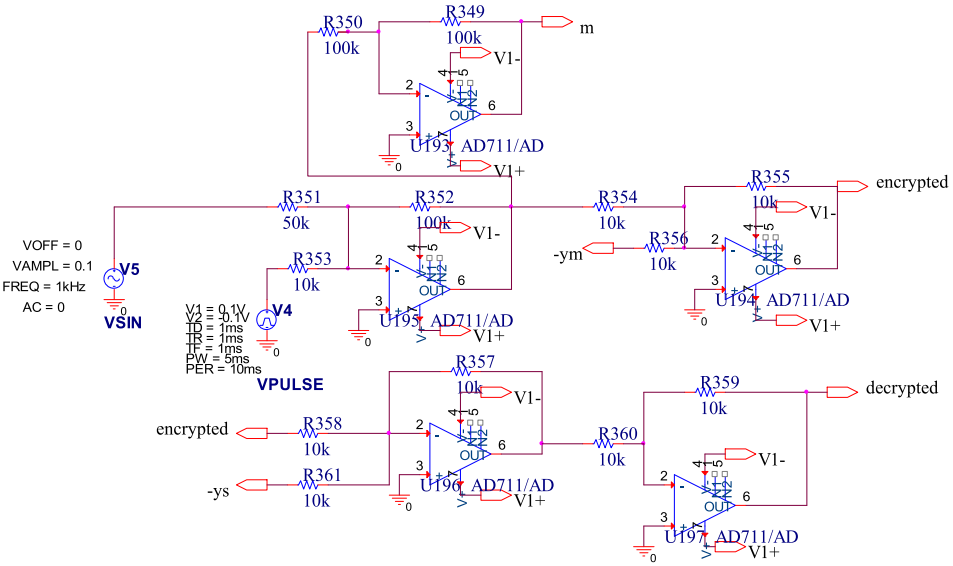

FIGURE 26. Secure communication structure.

Capture environments. Furthermore, an experimental study was implemented for electronic circuits with high precision of synchronization outputs. The archived outcomes exhibit the small overshoot of the synchronization tracking errors and small errors related to the states of the master and slave systems. In addition, the sent data in the master area and the recovered data in the slave area were mostly the same. The encrypted data were strongly different from the sent data, which confirms that the rescaled Chen chaotic system is usable as a secure communication system and that the proposed control algorithms are good for synchronization systems. This topic will be further explore in our near future work on secure communication with fractional-order T-S fuzzy chaotic systems. The results suggests that the fixed-time sliding mode, terminal sliding mode, or exponential convergence control designs can be further considered in electronics circuit experiment.

APPENDIX

This section is used to show the electronic circuits. See Figures 23–28.

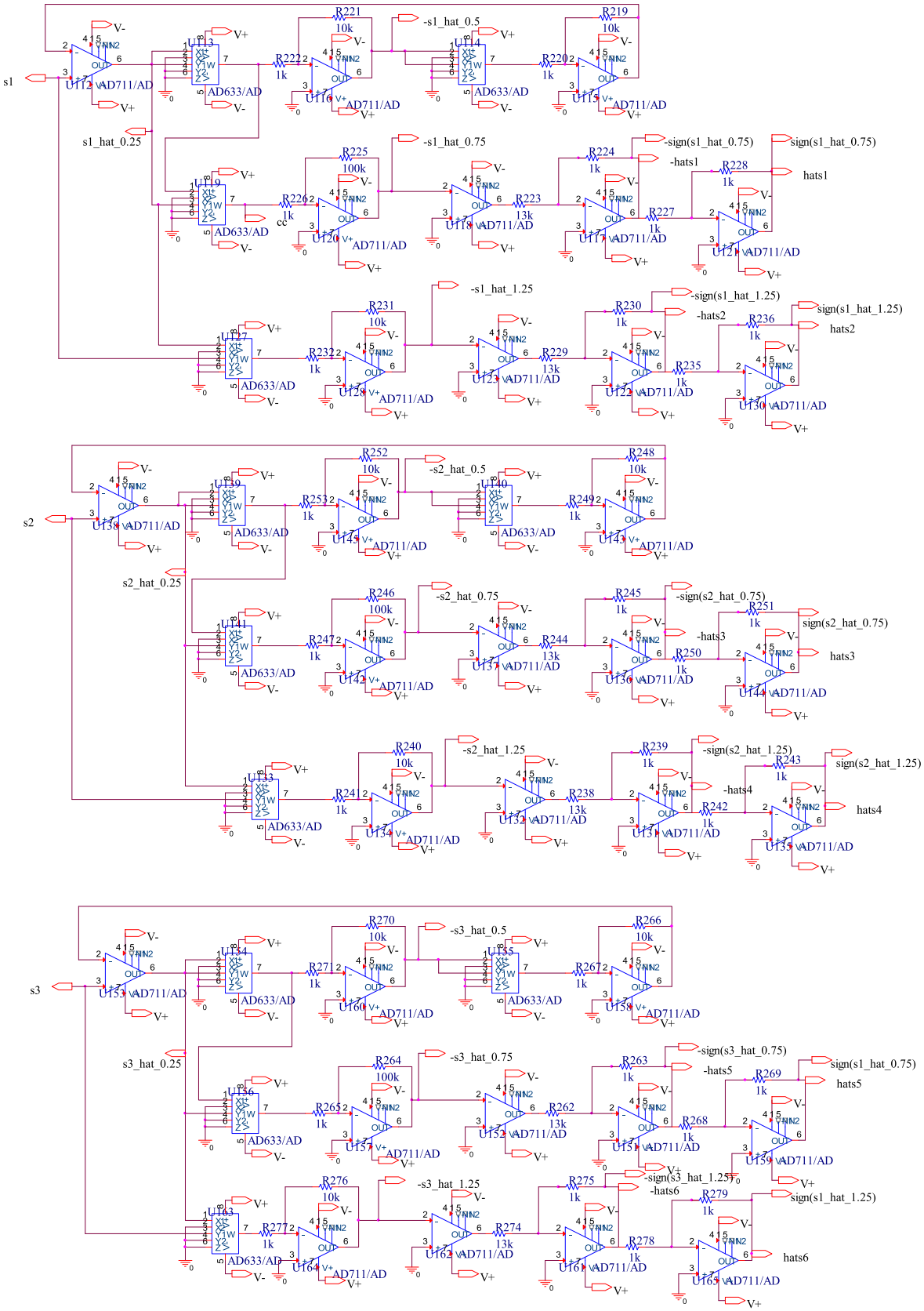

FIGURE 27. Sliding-mode control.

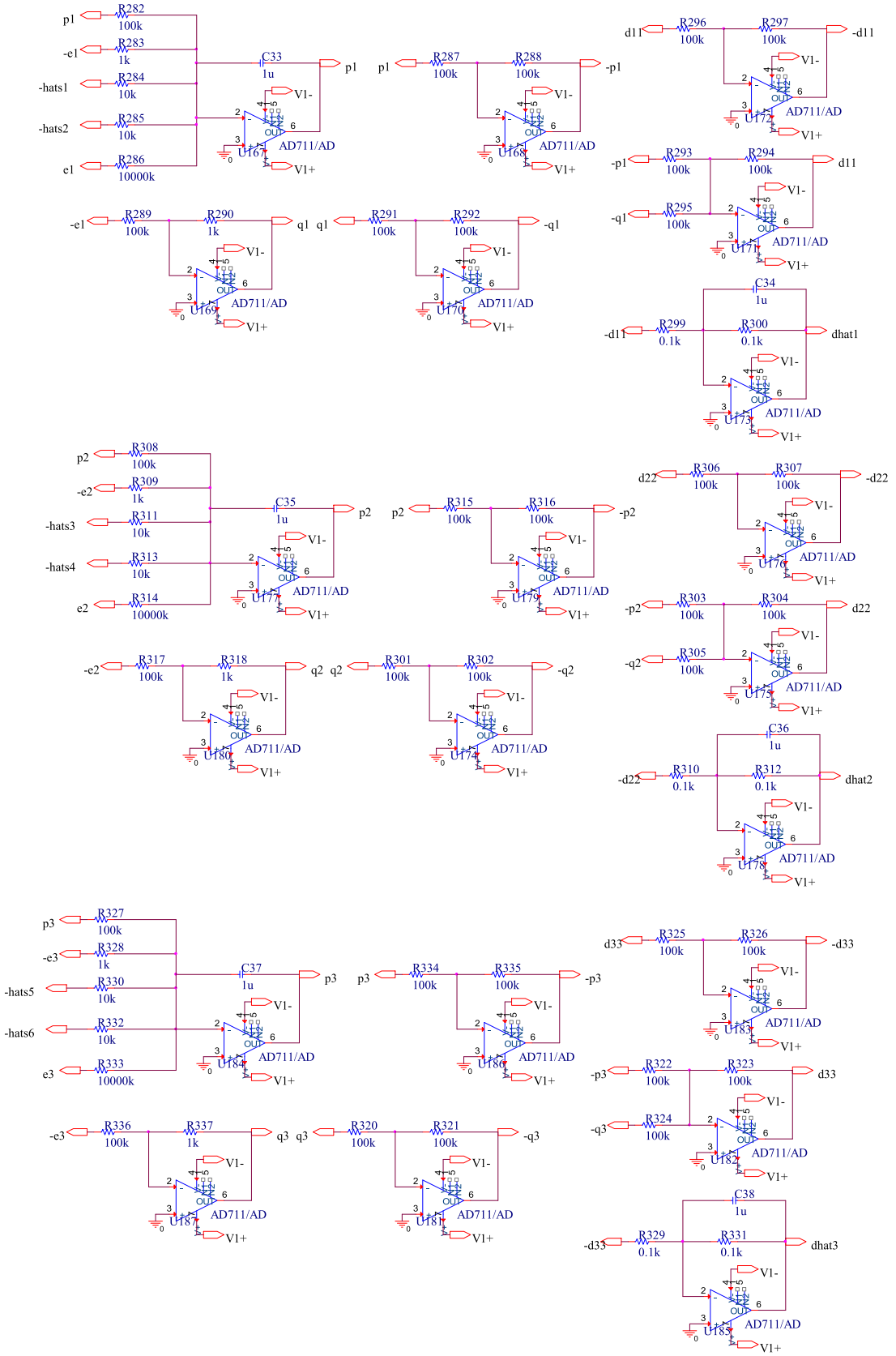

FIGURE 28. Disturbance observer structure.

REFERENCES

[1] Y.-J. Chen, H.-G. Chou, W.-J. Wang, S.-H. Tsai, K. Tanaka, H. O. Wang, and K.-C. Wang, "A polynomial-fuzzy-model-based synchronization methodology for the multi-scroll Chen chaotic secure communication system," *Eng. Appl. Artif. Intell.*, vol. 87, Jan. 2020, Art. no. 103251.

[2] S. Çiçek, U. E. Kocamaz, and Y. Uyaroğlu, "Secure communication with a chaotic system owning logic element," *AEU-Int. J. Electron. Commun.*, vol. 88, pp. 52–62, May 2018.

[3] V. N. Giap, S.-C. Huang, Q. D. Nguyen, and T.-J. Su, "Disturbance observer-based linear matrix inequality for the synchronization of Takagi-Sugeno fuzzy chaotic systems," *IEEE Access*, vol. 8, pp. 225805–225821, Dec. 2020.

[4] V. N. Giap, Q. D. Nguyen, and S. C. Huang, "Synthetic adaptive fuzzy disturbance observer and sliding-mode control for chaos-based secure communication systems," *IEEE Access*, vol. 9, pp. 23907–23928, 2021.

[5] C. S. Pappu, B. C. Flores, P. S. Debroux, and J. E. Boehm, "An electronic implementation of Lorenz chaotic oscillator synchronization for bistatic radar applications," *IEEE Trans. Aerosp. Electron. Syst.*, vol. 53, no. 4, pp. 2001–2013, Aug. 2017.

[6] B. Vaseghi, S. S. Hashemi, S. Mobayen, and A. Fekih, "Finite time chaos synchronization in time-delay channel and its application to satellite image encryption in OFDM communication systems," *IEEE Access*, vol. 9, pp. 21332–21344, Jan. 2021.

[7] M. Zhou and C. Wang, "A novel image encryption scheme based on conservative hyperchaotic system and closed-loop diffusion between blocks," *Signal Process.*, vol. 171, Jun. 2020, Art. no. 107484.

[8] Y.-Q. Zhang, J.-L. Hao, and X.-Y. Wang, "An efficient image encryption scheme based on S-boxes and fractional-order differential logistic map," *IEEE Access*, vol. 8, pp. 54175–54188, 2020.

[9] X. Wang and S. Gao, "Image encryption algorithm for synchronously updating Boolean networks based on matrix semi-tensor product theory," *Inf. Sci.*, vol. 507, pp. 16–36, Jan. 2020.

[10] S. Vaidyanathan, A. Akgul, S. Kaçar, and U. Çavuşoğlu, "A new 4-D chaotic hyperjerk system, its synchronization, circuit design and applications in RNG, image encryption and chaos-based steganography," *Eur. Phys. J. Plus*, vol. 133, no. 2, pp. 46–64, Feb. 2018.

[11] Y. Y. Wang, H. R. Karimi, and H. C. Yan, "An adaptive event-triggered synchronization approach for chaotic Lur'e systems subject to aperiodic sampled data," *IEEE Trans. Circuits Syst. II, Exp. Briefs*, vol. 66, no. 3, pp. 442–446, Mar. 2019.

[12] D. Chang, Z. Li, M. Wang, and Y. Zeng, "A novel digital programmable multi-scroll chaotic system and its application in FPGA-based audio secure communication," *AEU-Int. J. Electron. Commun.*, vol. 88, pp. 20–29, May 2018.

[13] V.-N. Giap, S.-C. Huang, and Q. D. Nguyen, "Synchronization of 3D chaotic system based on sliding mode control: Electronic circuit implementation," in *Proc. IEEE Eurasia Conf. IoT, Commun. Eng. (ECICE)*, Yunlin, Taiwan, Oct. 2020, pp. 156–159, doi: 10.1109/ECICE50847.2020.9301998.

[14] Z. Wu, X. Zhang, and X. Zhong, "Generalized chaos synchronization circuit simulation and asymmetric image encryption," *IEEE Access*, vol. 7, pp. 37989–38008, 2019.

[15] Q. Lai, B. Norouzi, and F. Liu, "Dynamic analysis, circuit realization, control design and image encryption application of an extended Lü system with coexisting attractors," *Chaos, Solitons Fractals*, vol. 114, pp. 230–245, Sep. 2018.

[16] L. Zhou and F. Tan, "A chaotic secure communication scheme based on synchronization of double-layered and multiple complex networks," *Nonlinear Dyn.*, vol. 96, no. 2, pp. 869–883, Apr. 2019.

[17] H. Lin, C. Wang, and Y. Tan, "Hidden extreme multistability with hyperchaos and transient chaos in a Hopfield neural network affected by electromagnetic radiation," *Nonlinear Dyn.*, vol. 99, no. 3, pp. 2369–2386, Feb. 2020.

[18] Z. Fei, C. Guan, and H. Gao, "Exponential synchronization of networked chaotic delayed neural network by a hybrid event trigger scheme," *IEEE Trans. Neural Netw. Learn. Syst.*, vol. 29, no. 6, pp. 2558–2567, Jun. 2018.

[19] P. Liu, Z. Zeng, and J. Wang, "Global synchronization of coupled fractional-order recurrent neural networks," *IEEE Trans. Neural Netw. Learn. Syst.*, vol. 30, no. 8, pp. 2358–2368, Aug. 2019.

[20] J.-L. Wang, Z. Qin, H.-N. Wu, and T. Huang, "Passivity and synchronization of coupled uncertain reaction-diffusion neural networks with multiple time delays," *IEEE Trans. Neural Netw. Learn. Syst.*, vol. 30, no. 8, pp. 2434–2448, Aug. 2019.

[21] Z. Chen, F. Huang, C. Yang, and B. Yao, "Adaptive fuzzy backstepping control for stable nonlinear bilateral teleoperation manipulators with enhanced transparency performance," *IEEE Trans. Ind. Electron.*, vol. 67, no. 1, pp. 746–756, Jan. 2020, doi: 10.1109/TIE.2019.2898587.

[22] Z. Chen, F. Huang, W. Chen, J. Zhang, W. Sun, J. Chen, J. Gu, and S. Zhu, "RBFNN-based adaptive sliding mode control design for delayed nonlinear multilateral telerobotic system with cooperative manipulation," *IEEE Trans. Ind. Informat.*, vol. 16, no. 2, pp. 1236–1247, Feb. 2020, doi: 10.1109/TII.2019.2927806.

[23] T. Takagi and M. Sugeno, "Fuzzy identification of systems and its applications to modeling and control," *IEEE Trans. Syst., Man, Cybern. B, Cybern.*, vol. SMCB-15, no. 1, pp. 116–132, Jan. 1985.

[24] K. Tanaka and H. Wang, *Fuzzy Control Systems Design and Analysis: A Linear Matrix Inequality Approach*. New York, NY, USA: Wiley, 2001.

[25] R. Sakthivel, R. Sakthivel, O. Kwon, and P. Selvaraj, "Synchronisation of stochastic T–S fuzzy multi-weighted complex dynamical networks with actuator fault and input saturation," *IET Control Theory Appl.*, vol. 14, no. 14, pp. 1957–1967, Sep. 2020.

[26] V.-P. Vu, W.-J. Wang, H.-C. Chen, and J. M. Zurada, "Unknown input-based observer synthesis for a polynomial T–S fuzzy model system with uncertainties," *IEEE Trans. Fuzzy Syst.*, vol. 26, no. 3, pp. 1447–1458, Jun. 2018.

[27] V. N. Giap, S.-C. Huang, Q. D. Nguyen, and T.-J. Su, "Robust control-based disturbance observer and optimal states feedback for T–S fuzzy systems," *J. Low Freq. Noise, Vib. Act. Control*, vol. 40, no. 3, Dec. 2020, Art. no. 1461348420981181.

[28] Q. Zhang, R. Li, and J. Ren, "Robust adaptive sliding mode observer design for T-S fuzzy descriptor systems with time-varying delay," *IEEE Access*, vol. 6, pp. 46002–46018, 2018, doi: 10.1109/ACCESS.2018.2865618.

[29] G. Q. Zhong and W. K. S. Tang, "Circuitry implementation and synchronization of Chen's attractor," *Int. J. Bifurcation Chaos*, vol. 12, no. 6, pp. 1423–1427, Jun. 2002.

[30] W.-H. Chen, "Disturbance observer based control for nonlinear systems," *IEEE/ASME Trans. Mechatronics*, vol. 9, no. 4, pp. 706–710, Dec. 2004.

[31] X. Wu, K. Xu, M. Lei, and X. He, "Disturbance-compensation-based continuous sliding mode control for overhead cranes with disturbances," *IEEE Trans. Autom. Sci. Eng.*, vol. 17, no. 4, pp. 2182–2189, Oct. 2020.

[32] A. T. Nguyen, B. A. Basit, H. H. Choi, and J.-W. Jung, "Disturbance attenuation for surface-mounted PMSM drives using nonlinear disturbance observer-based sliding mode control," *IEEE Access*, vol. 8, pp. 86345–86356, 2020.

[33] X. Liu, H. Yu, J. Yu, and Y. Zhao, "A novel speed control method based on port-controlled Hamiltonian and disturbance observer for PMSM drives," *IEEE Access*, vol. 7, pp. 111115–111123, 2019.

[34] V. Utkin, "Variable structure systems with sliding modes," *IEEE Trans. Autom. Control*, vol. AC-22, no. 2, pp. 212–222, Apr. 1977.

[35] Q. Zhang, J. Zhang, and Y. Wang, "Sliding-mode control for singular Markovian jump systems with Brownian motion based on stochastic sliding mode surface," *IEEE Trans. Syst., Man, Cybern. Syst.*, vol. 49, no. 3, pp. 494–505, Mar. 2019.

[36] C.-C. Fuh, "Variable-thickness boundary layers for sliding mode control," *J. Mar. Sci. Technol.*, vol. 16, no. 4, pp. 288–294, Dec. 2008.

[37] V.-N. Giap and S.-C. Huang, "Effectiveness of fuzzy sliding mode control boundary layer based on uncertainty and disturbance compensator on suspension active magnetic bearing system," *Meas. Control*, vol. 53, nos. 5–6, pp. 934–942, Mar. 2020.

[38] G. Gandikota and D. K. Das, "Disturbance observer–based adaptive boundary layer sliding mode controller for a type of nonlinear multiple-input multiple-output system," *Int. J. Robust Nonlinear Control*, vol. 29, no. 17, pp. 5886–5912, Aug. 2019.

[39] S. Wu, X. Su, and K. Wang, "Time-dependent global nonsingular fixed-time terminal sliding mode control-based speed tracking of permanent magnet synchronous motor," *IEEE Access*, vol. 8, pp. 186408–186420, Oct. 2020.

[40] V. H. P. Rodrigues, T. R. Oliveira, and J. P. V. S. Cunha, "Globally stable synchronization of chaotic systems based on norm observers connected in cascade," *IEEE Trans. Circuits Syst. II, Exp. Briefs*, vol. 63, no. 9, pp. 883–887, Sep. 2016.

[41] Y. Tian, Y. Cai, and Y. Deng, "A fast nonsingular terminal sliding mode control method for nonlinear systems with fixed-time stability guarantees," *IEEE Access*, vol. 8, pp. 60444–60454, 2020.

[42] A. Polyakov, "Nonlinear feedback design for fixed-time stabilization of linear control systems," *IEEE Trans. Autom. Control*, vol. 57, no. 8, pp. 2106–2110, Aug. 2012.
[43] H. Li and Y. Cai, "On SFTSM control with fixed-time convergence," *IET Control Theory Appl.*, vol. 11, no. 6, pp. 766–773, Apr. 2017.

VAN NAM GIAP received the B.S. degree in control engineering and automation from Hanoi University of Science and Technology, Hanoi, Vietnam, in 2015, the master's degree in electronic engineering from the National Kaohsiung University of Applied and Sciences, Kaohsiung, Taiwan, in 2017, and the Ph.D. degree in mechanical engineering from the National Kaohsiung University of Science and Technology, Taiwan, in June 2021. His research interests include sliding mode control, disturbance and uncertainty estimation, fuzzy logic control, secure communication, and magnetic bearing system and its applications.

HONG SON VU received the B.S. degree in electrical engineering from Hung Yen University of Technology and Education, Hung Yen, Vietnam, in 2008, the M.S. degree in automation engineering from Military Technical Academy, Hanoi, Vietnam, in 2011, and the Ph.D. degree from Feng Chia University, Taichung, Taiwan, in June 2016.

Since 2008, he has been with the Faculty of Electrical and Electronic Engineering, Hung Yen University of Technology and Education, as a Lecturer. He has published more than 17 refereed papers/articles in low-power VLSI architecture designs for visual/audio signal processing. His research interests include VLSI architecture design, system-on-chip design, object detection, electronic circuits, and active noise cancellation.

Dr. Vu was a recipient of the Excellent Award of MXIC Design Contest, Taiwan, in 2014.

QUANG DICH NGUYEN received the B.S. degree in electrical engineering from Hanoi University of Technology, Hanoi, Vietnam, in 1997, the M.S. degree in electrical engineering from Dresden University of Technology, Dresden, Germany, in 2003, and the Ph.D. degree from Ritsumeikan University, Kusatsu, Japan, in 2010. Since 2000, he has been with Hanoi University of Science and Technology, Vietnam, where he is currently an Associate Professor and the Executive Dean of the Institute for Control Engineering and Automation. His research interests include magnetic bearings, self-bearing motors, and sensor-less motor control.

SHYH-CHOUR HUANG (Senior Member, IEEE) received the bachelor's degree in aeronautics and astronautics engineering from National Cheng Kung University, Taiwan, in 1980, and the Ph.D. degree in mechanical engineering from the University of Cincinnati, Cincinnati, OH, USA, in 1990. He is currently a Professor of mechanical engineering at the National Kaohsiung University of Science and Technology, Taiwan. His research interests include micro-electromechanical systems' design, biomechanics, compliant mechanisms, multi-body dynamics, fuzzy logic control, vibration control, and optimization algorithms.